MICROSTRUCTURE AND MAGNETIC PROPERTIES OF Fe-Cr-15wt.%Co ALLOYS WITH AND WITHOUT V, V+Ti ADDITIONS

CONTENTS

MICROSTRUCTURE AND MAGNETIC PROPERTIES OF Fe-Cr-15wt.%Co ALLOYS WITH AND WITHOUT V, V+Ti ADDITIONS

YALCIN BELLI

Department of Materials Science,

Materials and Molecular Research Division,

University of California,

Lawrence Berkeley Laboratory;

Berkeley, California 94720.

ABSTRACT

The relationship between microstructure and magnetic properties of Fe-28Cr-15Co, Fe-23Cr-15Co-5V and Fe-23Cr-15Co-3V-2Ti (wt.%) alloys have been investigated by transmission electron microscopy, and Lorentz microscopy. The heat treatments adopted for the present investigation are 1) isothermal aging, 2) thermomagnetic treatment (TMT) + step-aging, and 3) TMT + continuous cooling. The morphology of the microstructure is very much affected by the aging temperature. Thermomagnetic treatment is very effective in elongation of the Fe-Co rich (α_1) phase particles, and the elongation of the α_1 phase particles is independent of crystal orientation. Step-aging and continuous cooling produce optimum magnetic properties. During step-aging microstructural features remain essentially unchanged, and the composition difference of the two phases increases. Continuous cooling is an alternative way to pro-

duce optimum magnetic properties. Microstructural features are almost independent of the cooling rate, and then they must be developed mainly by the TMT. Lorentz microscopy results show that the domain walls tend to lie in the weakly ferromagnetic matrix phase and are pinned by Fe-Co rich (α_1) phase particles as pinning sites (as opposed to the supposed single domain hardening). This observation suggests that the magnetization mechanism is governed by domain wall pinning. Magnetic domains are narrower in optimally treated alloys, and elongated parallel to the applied field. The anisotropy induced during TMT increases during step-aging or continuous cooling. The three alloys produce similar magnetic properties. However, due to their more facilitated heat treatments the alloys containing V and V+Ti additions would be of more industrial interest.

INTRODUCTION

Newly developed Fe-Cr-Co permanent magnet alloys have technologically become potential hard magnets due to their desirable magnetic properties combined with their good ductility.

Considering the magnetization mechanism, two types of magnets are produced for permanent magnet applications. The first one gains its magnetic properties by the pinning of domain wall motion by obstacles such as dislocations, inclusions and precipitates (e.g. magnet steels, Fe-Co-Mo (Remalloy), some rare earth magnets). The second one consists of small particles, below a critical diameter of which domain walls cease to exist. The change of the direction of magnetization requires the rotation of the magnetic moments of the single domain particles, which are embedded in non-magnetic matrix, and in this process no domain wall formation or motion takes place. The second one is usually considered to give much higher coercive forces than the first one. The required morphology for the second one can be obtained by either the dispersion of the strongly magnetic powder particles in non-magnetic matrixes (Lodex - magnets), or by producing a morphology of magnetic precipitate phase dispersed in a non -magnetic matrix by spinodal decomposition of a high temperature phase after aging inside the miscibility gap of the system. Alnico, Cu-Ni-Fe alloys fall into this second category.

Fe-Cr-Co permanent magnet alloys had been developed in 1971,[1] by extending the miscibility gap in the Fe-Cr system to the ternary Fe-Cr-Co system. It was found that the addition of Co increases the miscibility gap tempera-

ture of the Fe-Cr system.[1,2] The Fe-Cr-Co alloys have magnetic properties comparable to those of commonly used Alnico permanent magnets and are ductile enough to be cold worked and machined at certain stages of their production.[1] Alnico magnets are brittle, and usually cast or sintered to their final shape. It should be avoided for them to give sharp corners or complex thin shapes,[2,3] and their surface grinding is usually the only possible finishing operation. Due to the superior mechanical properties combined with desirable magnetic properties, the newly developed Fe-Cr-Co alloys offer the possibility of producing magnets or magnetic devices which are difficult to be manufactured from brittle Alnico alloys. Fe-Cr-Co alloys have replaced some commercial ductile magnets, such as Cu-Ni-Fe and Fe-Co-Mo (Remalloy).

The ternary Fe-Cr-Co alloys have some difficulties concerning their practical manufacturing. These are: 1) the necessity of solution treatment at high temperatures to obtain a single α phase, and 2) the necessity of fast quenching to prevent γ or σ-phase transformations.[4,5] An addition of Si to the ternary alloys was found to have desired effects on facilitating the heat treatment with desirable magnetic properties.[4] The addition of Mo to the alloys improves the magnetic properties, but it also stimulates the formation of embrittling σ-phase, deteriorating the mechanical properties. This is due to the fact that the so called α forming elements (Mo, W, V, Ti and Nb) also generally promote the σ-phase formation.[7]

The $\alpha+\sigma$ phase region in the "C" curve of the TTT (time, temperature, transformation) diagram for Fe-Cr-Co alloys can be shifted to lower tempera-

tu:es and longer aging times by lowering the Cr and Co content of the alloys.[8] Thus, the workability of alloys with low Cr and Co content are increased by preventing the σ-phase formation, although the magnetic properties of the alloys are lowered with lowering Cr and Co content. Thus, Fe-Cr-Co alloys with low Cr and Co content are produced because of practical production reasons even though they have somewhat less magnetic properties compared to the ones with higher Cr and Co content.

To overcome these difficulties, ternary alloys were modified by adding α forming elements for extending the α phase region to just above the miscibility gap. The modified alloys can be solution treated at low temperatures and the fast quenching rates are not necessary. The Fe-Cr-Co alloys were modified by Nb and Al additions in the alloys containing low Cr and Co content (25-30 wt. % Cr - 15 wt. % Co).[9] It was found that optimum magnetic properties can be produced by facilitated heat treatments such as continuous cooling because of the extension of the α phase region just above the miscibility gap. However, the Fe-Cr-Co-Nb-Al alloys were brittle in the as cast state.

As alternative magnets to Fe-Cr-Co-Nb-Al alloys, Fe-Cr-Co-V-(Ti) alloys were designed.[10] The alloys were ductile enough to be cold worked, machined or shaped in the as cast state /or after thermomagnetic treatment, with magnetic properties comparable to those of Alnico 5 magnets. The α-phase region of the Fe-Cr-15Co alloys are remarkably extended by the addition of 5 wt. % V, or 3 wt. % V - 2 wt. % Ti (see figures 1, 2 and 3). The solution treatment temperature of the alloys with V, V+Ti is very much lowered. Optimum magnetic

properties can be produced by facilitated heat treatments. McCaig[11] studied the magnetic stability of Fe-Cr-Co alloys and it was reported that the coercivity of the alloys generally falls slightly with increasing temperature, whereas for the alloys containing V and Ti the fall in coercive force does not commence until 300°C.

The magnetic hardening of the Fe-Cr-Co alloys is attributed to the spinodal decomposition of the high temperature stable (α) phase into a strongly magnetic Fe-Co phase (α_1) embedded in weakly or non -magnetic Cr-rich phase (α_2) upon aging inside the miscibility gap.[1,4-6,9-12] Therefore it is important to study the microstructural changes of the alloys with various heat treatments. And it has been thought that the high coercive force arises from the magnetic behaviour of the fine Fe-Co (α_1) phase particles.[1,4-6,9-12] However, no systematic analysis had been done on the magnetization reversal process.

The purpose of the present investigation is to study the relationship between microstructure and magnetic properties of Fe-Cr-15Co alloys without and with additions of V, V+Ti upon different heat treatments. Also a study of the magnetic domain structure of the alloys by transmission Lorentz electron microscopy (since magnetic hardening of the alloys occurs on a fine scale) is necessary in order to have a fundamental understanding of the magnetic hardening mechanism, which is necessary for further development of Fe-Cr-Co alloys.

II. EXPERIMENTAL PROCEDURE:

A. Alloy Preparation:

The chemical composition of the alloys used for the present investigation are;

Alloy A : Fe(balance) - 28Cr - 15Co (wt. %)

Alloy B : Fe(balance) - 23Cr - 15Co - 5V (wt. %)

Alloy C : Fe(balance) - 23Cr - 15Co - 3V - 2Ti (wt. %)

The alloys were prepared by melting 99.9% electrolytic Fe Cr and 99.9 - Co, V and Ti together, in an induction furnace under Argon atmosphere.

The alloys were placed in quartz tubes and filled with Argon. Alloy A was homogenized at 1250°C, alloys B and C at 1000°C for 12 hours and quenched in iced water by breaking the quartz tubes. The chemical composition analysis verified that the alloys are within 1% of the desired composition. The alloys were cut into 0.5mm thick samples and solution treated at 1350°C (alloy A), 1000°C (Alloys B and C) for one hour. These specimens were then used for microstructural analysis after the desired heat treatments.

The specimens for magnetic measurements were prepared by melting 99.9% electrolytic Fe and Cr, 99.5%Co Ferrovanadium, and Ferrotitanium in air. The melt was cast in quartz tubes with an inside diameter of 5mm. The ingots were cut into 30mm long bars and solution treated at 1300°C (Alloy A), 1000°C (Alloys B and C) for 1 hour. Following solution treatment they were thermomagnetically treated and step-aged or continuously cooled. The mag-

netic properties of the alloys were measured with an automatic recording flux meter. (These alloys were made at Tohoku University in Japan.) After that, thin sheet electron microscopy specimens (=10 mils) were cut from these bars parallel and perpendicular to the direction of the applied field (long axis of the specimens).

B. Electron Microscopy:

The thin sheet specimens were electrochemically /or mechanically thinned down to 5 mils, and the electron microscopy disc specimens were spark eroded. After thinning the disc specimens to 3-4 mils on a fine grinding paper (600 grit and finer), they were polished in an automatic jet polisher by using an electrolytic solution consisting of 23% perchloric acid ($HClO_4$) and 77% acetic acid (CH_3COOH). This process is preferentially thinning the Fe-Co (α_1) phase, in order to have the contrast difference between the two phases. Since the structure factors of the two phases are close to each other, the process of preferential thinning is necessary to have contrast difference between the two phases by having a thickness difference between the two phases, this thickness difference resulting in absorption difference.

In order not to change microstructural features by preferential etching, special attention should be paid during polishing. During the course of this investigation it has been observed that it is quite possible to change the microstructural features by preferential etching, and hence, misinterpret the microstructural features. To eliminate this problem, several specimens of the same heat treatment were made and observed. The JEM-7A and Phillips EM301

microscopes were used for microstructural analysis.

Transmission Lorentz Microscopy specimens were prepared and observed under the above considerations. Fresnel (out-of-focus) and Foucault (displaced-aperture) methods of Lorentz Microscopy[14,15] were used to image magnetic domain walls and domains. Hitachi-125, with a modified specimen holder which raises the position of the specimen by 3mm, Philips EM301, operating with objective lens off, and JEM-7A electron microscopes were used for Lorentz Microscopy. The defocus distance (z) was 20-45 microns. Exposure times varying from 1 to 5 minutes have been used.

III. EXPERIMENTAL RESULTS:

A. MICROSTRUCTURE:

a) Formation of Equilibrium Phases:

The bright field (B.F.) micrographs shown in figure 4 illustrate the microstructure of alloys A, B and C in as quenched state after solution treatment. These micrographs show that the alloys consist of single α phase after solution treatment. Due to the very high quenching rates, the formation of γ or σ-phases may have been avoided. However, in the specimens used for magnetic measurements the γ phase has been observed. Figure 5 illustrates the B.F. micrograph of the step-aged alloy C, shows a γ phase region which consists of small γ grains. The occurance of σ-phase was also observed during aging inside the miscibility gap B.F. and D.F. micrographs illustrated in figure 6, taken from the alloy A aged at 640°C for 1 hour, shows the σ-phase. Considerable amount of σ-phase has been formed within 1 hour at this temperature, although the σ-phase formation had been thought to be not critical at this relative low temperature. B.F. micrographs shown in figure 7 are taken from the alloy A thermomagnetically treated at 670°C, followed by step-aging. Figure 7(a) shows a morphology of three phase mixture; $(\alpha_1 + \alpha_2)$ grains having σ-phase along grain boundaries, and γ phase with dislocations. The σ-phase exhibits some cellular type of microstructure, which is shown with higher magnification in figure 7(b). This type of morphology of the σ-phase has also been observed in an Fe-31Cr-23Co (wt.%) alloy.[5] The absence of the elongated

particles near the grain boundaries may be due to localized change of composition along the grain boundaries. This morphology has been seen only in this particular step-aged alloy.

b) Isothermal aging:

The miscibility gap temperature for the alloys A, B and C has been found to be between 670°C and 680°C (680°C shows no decomposition). The reported miscibility gap temperature for the alloy A is 640°C,[16] and then the shape of the miscibility gap for the alloys A, B and C is not known at present.

Figure 8 illustrates the B.F. micrographs of the alloy B after aging for one hour at 660°C, 650°C, 640°C and 630°C, respectively. The phase with bright contrast is the Fe-rich phase (α_1) and the one with dark contrast is the Cr-rich phase (α_2).[17] These micrographs suggest that the morphology of the microstructure and the volume fractions of the two phases are very sensitive to the aging temperature, i.e., the lower the aging temperature, the finer is the (α_1) phase. These results are consistent with the expected miscibility gap shape which is quite asymmetric,[18] the α_1 phase appears as rod shaped particles which become interconnected after aging at 640°C.

The B.F. micrographs taken from the isothermally aged alloy A after aging for 1 hour at 670°C, 650°C and 640°C are illustrated in figure 9. Figure 9(a) implies that 670°C is very close to the top of the miscibility gap. These micrographs show similar features to those illustrated in figure 8, i.e., the morphology of the microstructure and the volume fractions of the two phases are very sensitive to the aging temperature. The morphology of the microstructure of

the isothermally aged alloy A at 650°C for 1 hour is very similar to that of alloy B aged at 660°C for 1 hour. However, the morphology of the microstructure of alloys A and B treated at 640°C is very similar. These results imply that the shape of the miscibility gap for the alloy A and B is not the same. This result is consistent with the experimentally found miscibility gap for Fe-Cr-15Co alloys after adding α forming elements (e.g. Nb and Al).[18]

These results are important in understanding the effect of thermomagnetic treatment (TMT) of the alloys at these temperatures. Isothermal aging itself fails to produce optimum magnetic properties of Fe-Cr-Co alloys even after prolonged aging times.[15-17]

c) Thermomagnetic treatment (TMT) and Step-aging:

It is well known that the thermomagnetic treatment plays an important role in producing good magnetic properties of Fe-Cr-Co and Alnico alloys.[1,5,10,17,20] During TMT, a field is applied along the long axis of the specimens. The α_1 phase particles formed under applied field are expected to be elongated parallel to the applied field direction, lowering its magnetostatic energy. In Fe-Cr-Co alloys TMT is more effective in improving the B_r (remanent induction) than H_c (coercive force).

The B.F. micrographs of alloy B, illustrated in figure 10 are taken from an isothermally aged specimen after aging at 650°C for 1 hour (a) without and (b) with TMT in a magnetic field of 2 KOe for 1 hour respectively. The effect of TMT treatment is seen clearly in figure 10(b) in that the α_1 phase is remarkably elongated along the direction of the applied field, whereas in figure 10(a)

the elongation of the α_1 phase is quite less and the dispersion of the particles seem to be random with a slight tendency for alignment along <100> directions due to the elastic anisotropy. The axial ratio of length to diameter ($m=l/d$) of the α_1 phase particles is ~ 1.7 in figure 10(a), whereas the axial ratio of the particles is ~3.5 after TMT (figure 10(b)). These results show that TMT is very effective in the elongation of α_1 particles parallel to the applied field direction.

It is reported that step-aging has beneficial effects in improving the magnetic properties of Fe-Cr-Co alloys, and that optimum magnetic properties can be obtained by the step-aging method.[5,10,17] After solution treatment the alloys are thermomagnetically treated to develop their microstructural features and then the alloys are step-aged at lower temperatures to increase the composition difference between the two phases. Five different temperatures of TMT were chosen to investigate the effects of the TMT temperature on the microstructure and the magnetic properties of the alloys. After TMT the alloys were step-aged at 620°C (except the one thermomagnetically treated at 630°C), 600°C, 580°C, and 560°C for 1 hour and subsequently aged at 540°C for 5 hours. A schematic diagram of step-aging is illustrated in figure 11.

The magnetic properties (i.e. ${}_iH_c$ (coercive force), B_r (remanent induction) and $(BH)_{max}$ (energy product)) of the step-aged alloys A, B and C as a function of the temperature of the TMT temperature are plotted in figures 12,13, and 14, respectively. The coercive force (${}_iH_c$) of the alloys are very much affected by the temperature of the TMT. Remanent induction (B_r),

which reflects the alignment of the Fe-Co (α_1) phase particles parallel to the applied field during TMT, remains almost constant. The energy product $(BH)_{max}$ varies due to the variation in the coercive force of the alloys. These variations in magnetic properties can be understood by analysis of the corresponding microstructures as discussed below.

Figure 15 illustrates the B.F. micrographs of the step-aged alloy B after different thermomagnetic treatments at (a) 660°C (H_c~420 Oe), (b) 650°C (H_c~520 Oe), (c) 640°C (H_c~370 Oe) and (d) 630°C (H_c~80 Oe), respectively. For example, figure 15(a) shows two morphologies of the α_1 phase viz., elongated α_1 phase particles, 300A° in diameter, and spherical α_1 particles 135A° in diameter. Since the larger α_1 phase particles are elongated, they should be formed during thermomagnetic treatment, whilst the small α_1 must be nucleated after TMT. These morphologies are produced when the step-aging interval (ΔT) between $T_{step\ n} - T_{step\ n-1}$ is large[17]. Figure 15(b) corresponding to the optimum magnetic properties shows the α_1 phase, approximately 300A° in diameter and 1200A° in length giving an aspect ratio of ~4. In figure 15(c) and 15(d), the particle diameters are about 200A°, 140A°, and the lengths about 400A° and 220A° respectively. The fine spherical particles are absent in figure 15(c) and 15(d). This is believed to be due to the fact that the step-aging interval is small.

The B.F. micrographs shown in figure 16 are taken from the step-aged alloy A after different TMT at (a) 670°C (H_c~240 Oe), (b) 660°C (H_c~610 Oe), (c) 650°C (H_c~580 Oe), and (d) 640°C (H_c~330 Oe), respectively. In

figure 16(a) two morphologies of the α_1 phase are also seen. The spherical α_1 phase is around 70A° in diameter, elongated α_1 phase is approximately 330A° in diameter. Figure 16(b) shows the same morphology where the spherical α_1 phase particles are around 180A°, and the elongated α_1 phase is 285A° in diameter. These particles are absent in figure 16(c) and 16(d), where the particle sizes become smaller as in alloy B. Again these morphologies are produced when the step-aging interval ΔT is large, being ≥ 40°C for alloy A.

Figure 17 illustrates the B.F. micrograph of the step aged alloy C after thermomagnetic treatment at (a) 660°C ($H_i \sim 550$ Oe), (b) 650°C ($H_i \sim 580$ Oe), (c) 640°C ($H_i \sim 390$ Oe), and (d) 630°C ($H_i \sim 150$ Oe), respectively. This alloy exhibits very similar microstructural features as alloy B does. Figure 17(a) shows secondary α_1 particles around 130A° in diameter. Secondary α_1 particles are also seen in figure 17(b) which are around 175A° in diameter. The secondary particles are absent in figures 17(c) and 17(d), where the particle sizes becomes smaller as it is found in the isothermally aged alloys at these temperatures.

Figure 18 shows the B.F. micrograph of alloy B thermomagnetically treated at 650°C for 2 hours and aged at 540°C for 18 hours. The step-aging interval (ΔT) is 110°C for this alloy. Fine secondary decomposition is seen in the micrograph. Due to the asymmetry in the miscibility gap α_1 phase is now the major phase. The α_2' phase particles are around 15A° in diameter. This secondary decomposition may have occured spinodally, since the ΔT is so large that the α_2 phase may be located inside the spinodal upon aging at low tempera-

tures.

d) Continuous Cooling:

As discussed in the previous part, optimum magnetic properties can be produced by the step-aging method. However, step-aging process is not industrially attractive. Consequently a continuous cooling process was developed for the alloys B and C to alter the step-aging. Figure 19 shows the schematic diagram of the continuous cooling method. The alloys are continuously cooled to TMT temperature after the solution treatment. In order to study the effects of continuous cooling rate on the magnetic properties and their microstructures, the alloys were thermomagnetically treated at 650°C (since 650°C is the best temperature for thermomagnetic treatment for alloys B and C), then continuously cooled to 540°C at the rates of 0.25°C-1°C/minute. The magnetic properties of continuously cooled alloys B and C as a function of cooling rate are given in figures 20 and 21, respectively. The coercive force ($_iH_c$) of the alloys increases with slower cooling rates, the rate of increase in ($_iH_c$) being lower at lower cooling rates. Remanent induction (B_r) remains practically constant. The variation in the energy product ($(BH)_{max}$) is due to the change in coercive force. Figure 22 shows the B.F. micrographs of the alloy B continuously cooled at the rates of (a) 1°C/min. (H_c~220 Oe), (b) 0.25°C/min. (H_c~520 Oe). These micrographs exhibit very similar features, such as the size and shape of the α_1 phase and its volume fraction. In figure 22(a) and 22(b) the rod diameter is about 300A°, 340A° and the length is about 690A° to 740A°, respectively. These micrographs suggest that the morphology of the microstructure

appears to be very similar, almost independently of the cooling rate. Since both specimens have the same TMT the morphology of the microstructure should be established during TMT.

Then in order to further examine the difference in microstructures of figures 22(a) and (b), a simple experiment was done as follows; both specimens are further aged at 540°C subsequent to continuous cooling. The coercive force of the fast cooled (1°C/min.) specimens can be remarkably increased from 220 Oe to 520 Oe, i.e., by a factor of more than 2, by isothermally aging the material at 540°C for 14.5 hours subsequent to continuous cooling. The increase in the coercive force of the optimally cooled alloys (0.25°C/min.) is very moderate (70 Oe) by the same heat treatment. Figure 23 illustrates the B.F. micrographs of the alloys B and cooled at a rate of 1°C/min. to 540°C, and aged at 540°C subsequent to continuous cooling. There is no noticeable difference in the morphology of the continuously cooled alloy B (figure 22(a)), and low temperature aged alloy B after continuous cooling (figure 23(a)). Figure 23(b) taken from the low temperature aged alloy C exhibits similar features. The low temperature aging of the fast cooled alloys (1°C/min.) does not essentially change the microstructure as it is found for Alnico alloys[20]. These results imply that compositions of the two phases differ depending on the continuous cooling rate, giving different coercive forces. Therefore, there are two alternative methods to produce the optimum properties in these alloys. One is by continuous cooling at a rate of 0.25°C/min. The other is by cooling at a rate of 1°C/min. and subsequently aging at low temperatures for long times.

B. OBSERVATION OF MAGNETIC DOMAINS:

In this section, the results of the Lorentz microscopy analysis on the structure of magnetic domains in the modulated structures ($\alpha_1+\alpha_2$) will be described. Figure 24 shows the Fresnel (out-of-focus) micrographs of the isothermally aged alloy B at 650°C for 1 hour where both phases are ferromagnetic with close saturation magnetization (M_s) values. The domain walls are straight, showing closure type domain structure. Figure 25 illustrates the Fresnel micrographs taken from the isothermally aged alloy C at 650°C for 1 hour. These micrographs show that the domain features of alloy C are similar to those in alloy B (figure 24). From these micrographs it is uncertain where the domain wall exactly lies. To answer this question the alloy was over-aged for 50 hours at 650°C, coarsening the α_1 phase particles from $\sim$150A° to $\sim$900A° in diameter. Magnetic domain walls and domains in this alloy are seen in figures 26(a) and 26(b), respectively. These micrographs show that the domain walls lie within the α_2 matrix phase, and they lie along <100> directions due to crystal anisotropy. This stems from the fact that the domain wall energy of the α_2 phase is lower than that of the α_1 phase. Domain walls in figure 26(a) are curved around the α_1 phase. These micrographs suggest that the domain walls which lie in α_2 are pinned by the more strongly magnetic α_1 particles. Further evidence of pinning of the domain walls by strongly magnetic α_1 phase particles is illustrated in figure 27. In figure 27(a) the domain wall with black contrast (divergent wall) lies within the weak ferromagnetic α_2 matrix phase and is curved around the α_1 phase particles. After photographing

the domain wall in figure 27(a) the specimen is tilted in order to alter the effective magnetic field acting on the specimen, and it was observed that the domain wall made a jump and was stopped by the α_1 phase particles at the position which is photographed and illustrated in figure 27(b). In figure 27(b) the domain wall still exists in the α_2 phase and is slightly bent around the α_1 phase particles. (several more jumps of the same domain wall were photographed and the same results outlined above were observed). These micrographs substantiate that domain walls which lie in the weaker ferromagnetic phase are pinned by the more strongly magnetic α_1 phase particles. It is concluded that for the isothermally aged alloys and also for alloys where both phases are ferromagnetic, the magnetization process of the alloys controlled by domain wall pinning (as opposed to single domain hardening where no domain walls and domain wall motion is involved), as the α_1 phase particles acting as pinning sites. A similar mechanism has also been proposed for $Sm(Co,Cu,Fe)_7$ magnets.[12]

Magnetic domain walls and their configuration for the alloy B are seen in figure 28 after thermomagnetic treatment at 650°C for 1 hour. Figure 28(a) shows the domain configuration parallel to the applied field of the alloy. Domain configurations are similar to those obtained from isothermally aged alloys. The main difference is that the domain walls lie parallel to the <100> directions in isothermally aged alloys whereas the domain walls usually lie parallel to the applied field in thermomagnetically treated alloys. Figure 28(b) shows the domain configuration of the same alloy in a foil perpendicular to the applied field. The domain configuration looks like those obtained from the

basal planes of the uniaxial cobalt alloys.

As discussed previously, (sections III.c and d) the alloys, either step-aged or continuous-cooled, produce optimum magnetic properties by enlarging the difference between the composition of the two phases. This will lead to an increase in the difference between the saturation manetization intensities of the two phases, without altering the microstructural features developed during the thermomagnetic treatment. Then it is interesting to see how the domain configurations change after continuous cooling and step-aging. Figure 29 illustrates the Foucault (displaced aperture method) micrographs of the alloy B continuously cooled at a rate of 1°C/min. ($H_c \sim 220$ Oe). The main features of the domain structure of the alloy are somewhat similar to those obtained from thermomagnetically treated alloys. However, the domain bands are narrower, and the domains are elongated parallel to the applied field, i.e., the direction in which α_1 phase particles are elongated. The domain configuration of the alloys given the optimum magnetic properties are different from those outlined above.

Figure 30 (a) and (b) are the Fresnel micrographs of the optimally step-aged alloy, showing the domain walls, and figure 31 (c) and (d) are the Foucault micrographs showing the magnetic domains. The observed domain walls are not straight, but curved. The magnetic domains are $0.5\mu m$ wide on the average, and are elongated parallel to the applied field. Their size is smaller than the isothermally aged or thermomagnetically treated alloys or fast continuous cooled alloy (figure 29). The Foucault micrograph illustrated in figure 31 shows these features more clearly at a higher magnification. The domains with

bright and dark contrast are elongated in the direction of the applied magnetic field (the direction in which the α_1 phase is elongated) as seen in this micrograph. The domains with black contrast are approximately 1500A° wide on the average. These observations suggest that the magnetic anisotropy is introduced parallel to the applied magnetic field after thermomagnetic treatment and step-aging. This induced anisotropy is known to be independent of the crystallographic orientations of individual grains, that is α_1 phase particles are elongated along the same direction independent of crystal orientation. Figure 32 illustrates these features clearly, that the domains are elongated parallel to the same direction in two grains having different crystal orientations.

A Fresnel micrograph of the optimally step-aged alloy B and the interpretation of its domain configuration are illustrated in figure 33. The Fresnel micrograph shows some larger domain bands parallel to each other, and some smaller domains approximately 2000A° wide in the large domain bands whose magnetization vectors are opposite (as illustrated more clearly in the figurative drawing). Also, there exists some smaller domains exhibiting the so called magnetization ripple structure in one dimension, indicating local variations of the M_s (saturation magnetization) direction. Figure 34 illustrates the Fresnel micrographs taken from the optimally step-aged alloy C in a section perpendicular to the applied field and shows the domain structure of a uniaxial ferromagnet. The domain structures look very similar to those obtained from the sections parallel to the applied field. Comparison of figure 34(a) and (b) with figure 28(a) shows that the change in domain configuration after step-aging in sections

perpendicular to the applied field is very similar to those observed in sections parallel to the applied field. However, the domain configurations taken from the sections perpendicular to the applied field might not represent those in the bulk material, since, the induced anisotropy perpendicular to the plane of the foil might have been changed for the thin foil electron microscopy specimens.

The domain wall thickness calculations in the alloy could give useful information about parameters which are necessary to discuss the magnetization reversal process of the alloy. Hence, the domain wall thickness measurements are done on the alloys given optimum magnetic properties. It is reported that divergent types of wall images (with dark contrast) are considered to be more accurate for domain wall thickness calculations using the geometrical theory of Lorentz microscopy.[15] Thus the width of divergent type of wall images in figures 30(a) and (b) was measured by microdensitometer analysis. The projected widths of the domain walls are found to be very nonuniform, varying from 840A° to 1510A°, almost by a factor of two, although the foil thickness appears to be uniform. This large deviation is thought to be due to the magnetic inhomogeneity of the specimen (strongly magnetic α_1 phase and weakly magnetic α_2 phase). Therefore, there is a large possibility that the electron beam may be deflected several times through the foil, depending on the distribution of the two phases in that particular area, thus giving different projected widths.

IV. DISCUSSION:

A. MICROSTRUCTURE:

a) Formation of Equilibrium Phases:

All three alloys A, B and C mainly consist of single α phase in their as quenched states. γ phase has been observed in the specimens used for magnetic measurements, which may have formed during quenching. More γ grains are seen for the continuously cooled alloys that are cooled slowly to the TMT temperature. From the magnetic and mechanical properties point of view σ phase formation is undesirable. The formation of the σ phase during quenching is prevented by lowering the Cr and Co contents. However, the formation of the σ-phase again becomes critical upon aging inside the miscibility gap. This may lead to serious amount of σ-phase formation in short times, as observed in an Fe-31Cr-23Co alloy.[5] The formation of the σ phase is more critical for the alloy A, than for the alloys B and C where only a small amount of σ phase is observed upon aging for 1 hour inside the miscibility gap. The metastable section diagrams, figures 1, 2 and 3, for the alloys A, B and C are constructed after aging the alloys in vacuum for 1 hour at temperatures of 600°C to 1200°C followed by quenching in water.[10] For the alloys B and C, from figures 2 and 3, γ or σ should not be formed during quenching or isothermal aging at 670°C - 640°C for 1 hour. However, γ or σ phases are present as shown by the electron microscopy results. In the light of these results, the validity of figures 1, 2 and 3 is questionable.

b) Isothermal Aging and TMT:

The morphology of the microstructure resulting from isothermal aging shows that microstructural features of the alloys are very sensitive to the aging temperature and volume fraction of the two phases. The α_1 phase particles appear as spheres at 670°C, becoming rod-like particles at 660°C and 650°C. The α_1 phase particles become interconnected at 640°C. The change in the volume fraction of the two phases are due to the large asymmetry in the shape of the miscibility gap. Alloys A and B show similar morphologies. However, the particle morphology and the volume fractions of the two phases are different. These results indicate that the alloys have somewhat different shapes of the miscibility gap. The decomposition process appears to be isotropic in the alloys during at least aging for 1 hour at temperatures 670°C to 630°C. The isotropic nature of the decomposition is due to the small misfit between the two phases.[5]

As it is shown in section III.A.c, thermomagnetic treatment is very effective in producing elongated α_1 phase particles parallel to the applied field. This elongation is by about a factor of two larger than in the case without TMT. That is the axial ratio of the α_1 phase is 1.7, after aging at 650°C for 1 hour, whereas the axial ratio is around 3.5 after thermomagnetic treatment at the same temperature. The elongation of the α_1 phase in these alloys is better than in the alloys used for previous investigations.[5,17]

The effects of an applied magnetic field on the microstructure of spinodally decomposing alloys was theoretically examined by Cahn[24] for the early stages of

spinodal decomposition. He considered that the two main sources of anisotropy are the magnetostatic and elastic energy. The magnetostatic energy favours the concentration waves parallel to the magnetic field, whereas the elastic anisotropy favours waves of certain crystallographic directions depending on the anisotropy of the crystal. He concluded that if the anisotropy in magnetostatic energy is very much larger than the elastic anisotropy energy, the decomposition mechanism ignores the crystallographic structure and gives plane waves whose superposition resembles two phases of rods parallel to the magnetization. If the elastic anisotropy exceeds the magnetic anisotropy then those waves of the favoured crystallographic orientation that are close to being parallel to the applied magnetic field, are preferred. He also concluded that the anisotropy in elastic energy usually by far exceeds the anisotropy of the magnetostatic energy, except near the Curie temperature of the original homogeneous alloy. Therefore, the parameters which control the magnitude of the elastic anisotropy i.e. 1) η^2 ($\eta = d\ln a / dc$), where a is the lattice parameter, and 2) ΔY (the spread in elastic constant Y for various orientations) should be chosen to be small. Since the decomposition process appears to be isotropic for 1 hour, the thermomagnetic treatment is very effective in the elongation of the particles. If the thermomagnetic treatment time is extended, the elastic anisotropy energy may exceed the magnetostatic anisotropy. In such a case the particles grow along <100> directions. For an Fe-31Cr-23Co alloy this is found to happen after TMT for 3 hours at 640°C.[17]

c) Step-aging:

As it is shown the optimum magnetic properties can be obtained by step-aging. The coercive force of the thermomagnetically treated alloys is very much increased by step-aging, whereas the increase in the remanence is moderate. The morphology of the α_1 phase established by the temperature of the thermomagnetic treatment remains essentially unchanged. Therefore the increase in coercivity during step-aging is believed to be associated with a change in composition of the two phases that results in an increase in the difference between the saturation magnetization intensities of the two phases. The same results have been obtained on other Fe-Cr-Co alloys in which the steps of the step-aging process are analyzed by Curie temperature measurements of the α_2 phase, and the temperature dependence of the magnetic properties.[6,17] The composition of the two phases change as the temperature is stepped down because the concentration of the Cr atoms in Fe-Co rich phase (α_1) decreases, and moreover the concentrations of the Fe and Co decreases in the Cr-rich phase being due to the shape of the miscibility gap. This enhancement of the composition differences between the two phases takes place by diffusion for small ΔT. However, if the step-aging interval is large, secondary decomposition takes place due to the increased supersaturation of the α_2 phase and the increased undercooling. This can be further explained as below. The free energy to create a homogeneous spherical nucleus (assuming that the composition of the phase falls in the nucleation and growth region) is given by[25]

$$\Delta G^* = \frac{16\pi\gamma^3}{3(\Delta G_V)^2} \quad \propto \quad \frac{\gamma^3}{(\Delta T)^2}$$

where γ is the surface energy between the nuclei and the decomposed phases, ΔG_v free energy change per unit volume, ΔT is the degree of undercooling [or $T_{step\,2} - T_{step\,(n-1)}$]. The larger the undercooling ΔT the smaller the fluctuation in free energy required to create a new particle. When ΔT is small, ΔG^* is large, therefore no new particle formation takes place. Thus the composition of the two phases changes by diffusion without changing the morphology of the microstructure. Similar observations are made in Alnico, Al-Ni and Fe-Cr-Co alloys.[26,5]

The secondary decomposition may take place spinodally provided that ΔT is large enough that the second step is inside the spinodal. If this happens the morphology of the secondary decomposed phases differs from the initial one, due to the asymmetry in the miscibility gap. The formation of secondary particles may deteriorate the magnetic properties, since some of the small secondary particles may behave superparamagnetically.[27]

d) Continuous Cooling:

This method is an alternative method to produce optimum magnetic properties for the alloys B and C, being industrially more attractive than step-aging. Optimum magnetic properties can be produced in two ways.

1) By cooling the specimens with the optimum cooling rate (0.25 °C/min.) or
2) By cooling the specimens at relatively higher rates and aging them at low temperatures subsequent to the continuous cooling.

However, the faster the cooling rates the longer the isothermal aging time

would be. The microstructural features of the optimally cooled and fast cooled specimens are very similar, indicating that only the composition of the two phases differs with different cooling rates. These results imply that the microstructural features are established by high temperature treatments, i.e., during thermomagnetic treatment, as it is found for Alnico alloys.[21] The low temperature aging treatment does not change the morphology but alters only the composition of the two phases. This is also similar to those observed in Alnico alloys.[26]

B. MAGNETIZATION REVERSAL PROCESS:

The domain configuration of the alloys changes upon different heat treatments. The domain walls lie parallel to the <100> directions in the alloys which have not had TMT. TMT induces anisotropy parallel to the applied field, and results in a change in domain configuration. The domain configuration of the alloys changes as the coercive force increases. The increase in composition difference between the two phases affects the domain configuration, viz., domain bands become much narrower and elongated parallel to the applied field. The anisotropy induced during TMT increases during step-aging or continuous cooling. The correlation between the domain structure and coercive force is that the domain bands get narrower as the coercive force increases and are elongated parallel to the direction of elongation of the α_1 phase particles.

As it is briefly discussed in the introduction, the magnetization reversal mechanism of Fe-Cr-Co alloys was thought to be due to single domain behaviour of the strongly magnetic Fe-Co phase (α_1) embedded in a weakly or

non -magnetic Cr-rich (α_2) phase during step-aging process.[6,12] Therefore the main idea of step-aging was to create a non-magnetic matrix, since the presence of a magnetic matrix would reduce the coercive force of the alloys due to the interactions between the particles. Cremer et al.[6] argue that the coercive force would be given by the empirical formula below:

$$_{I}H_{c} = p(1-p)\,(N_b - N_a)\,(I_{s_1} - I_{s_2})^2/I_s$$

where p is the packing fraction of the α_1 phase, N_b is the demagnetizing coefficient along the long axis, N_a is the demagnetizing coefficient along the short axis, I_{s_1} is the saturation magnetization of the α_1 phase, I_{s_2} that of the α_2 phase, and I_s is the saturation magnetization of the sample. As is seen from the equation above the presence of a ferromagnetic matrix will reduce the coercive force of the alloys depending on its I_{s_2} value. Therefore the coercive force of the step-aged specimens having magnetic matrixes would be lower. The coercive force of the Alnico alloys was also interpreted in this way.[26,28]

In spite of the interpretation of the origin of the coercive force of Alnico alloys by fine particles theory, domain walls have been observed in these alloys.[1,2] Later, these domain walls were explained as "interaction domains", which are attributed to magnetostatic interaction between single domain particles, and there are no domain walls in the normal sense between the domains.[34] These interaction domains are also reported for some Alnico alloys which have magnetic matrixes and the authors concluded that no direct correlation can be made between the domain structure and coercivity.[5]

The results of the present investigation, as outlined in section 3.B, have shown that domain walls exist after aging the material inside the miscibility gap to produce optimum magnetic properties. The analysis of these domain walls have shown that, these domain walls are the usual Bloch type walls and lie within the α_2 matrix, where the domain wall energy is lower and are pinned by the strongly magnetic α_1 phase particles where the domain wall energy is higher. This should be the magnetization reversal process of the alloys as long as the two phases are ferromagnetic. This may easily be the case for Alnico alloys which have magnetic matrixes. These results have shown that the coercive force of the specimens having magnetic matrixes can no longer be interpreted by single domain theory since the magnetization reversal process is found to be domain wall pinning as opposed to single domain hardening. Fe-Cr-15Co alloys with very close compositions and heat treatments are found to have weakly magnetic matrixes by Mössbauer Spectroscopy.[34] Therefore the magnetic properties of the alloys at optimum magnetic property conditions should be obtained by domain wall pinning.

Therefore the differences in the coercive forces of the alloys upon different heat treatments should be interpreted by the parameters which control the domain wall particle interaction, viz., parameters which determine the coercive force of the alloys.

Kersten[35] has considered the domain wall pinning case for non-magnetic inclusions, and calculated the parameters which controlled the coercive force. He treated many cases for various shapes and sizes of inclusions and the thick-

ness of the domain walls with respect to inclusions assuming a cubic array of inclusions. For the present work Kernsten's formula can be modified to treat the domain wall pinning by magnetic particles, that is, to include $(\gamma_1 - \gamma_2) = \Delta\gamma$ in his equations where γ_1 is the wall energy of the α_1 particles and γ_2 is the wall energy of the Cr-rich (α_2) matrix phase, where the domain walls lie. However, Kernsten's formula is very simplistic due to the fact that it considers a very regular distribution. It would not be realistic to use Kersten's model to interpret the coercive force differences of the alloys, since there exists size, shape and periodicity distribution in the alloys.

Schwabe[36] has treated the domain wall pinning model for magnetic and non-magnetic particles whose dimensions are small compared to domain wall thickness, δ. He also pointed out that for magnetic particles having axial ratio of more than $\simeq$ 1.04 the difference in wall energy will be smaller than the magnetostatic energy of the particles and can be neglected. That is, the energy required to rotate the M_s (saturation magnetization) vector of the elongated particles will much exceed the difference in wall energy which acts as a barrier to domain wall motion. Schwabe, therefore, assumes that in the case of elongated ellipsoidal particles the axial ratio of the particles is important, viz., the greater the axial ratio the higher the coercive force would be. However, for Fe-Cr-Co alloys it is well known that the difference in the coercive force with and without TMT is negligible,[1,5,6] viz., the elongation and the alignment of the particles does not essentially change the coercive force. Thus, Schwabe's model does not seem to be applicable, either. However, his model has

different statistical multipliers for the random distribution case (all domain walls are not parallel to the particles). His calculated statistical distribution does not apply for the present morphology. As the results of the present investigation have shown the domain walls lie parallel to the direction in which particles are elongated for the thermomagnetically treated alloys, and more pronounced at optimum magnetic property conditions. However the domain walls lie parallel to the <100> direction due to the crystal anisotropy, for the alloys that did not have TMT. Therefore in the second case the statistical calculations of the particles with respect to domain walls, whether their long axis lie parallel or perpendicular to the domain walls, will be of importance to determine the magnetic properties since it may explain the unaltered coercive force with and without TMT.

In the light of the present investigation the effects on the coercive force of the various parameters seem to be as follows. For the continuously cooled alloys it is found that the coercive force differs very much upon different cooling rates although the morphology of the microstructure is essentially the same. Also the coercive force of the fast cooled specimens can be increased upon aging at low temperatures subsequent to continuous cooling. This heat treatment does not change the morphology of the microstructure but increases the coercive force of the fast cooled specimens by a factor of more than two. These results imply that the composition difference between the two phases is a controlling parameter for the coercive force. Since microstructural features remain essentially the same, their effect on the coercive force cannot be concluded from the results above.

As discussed earlier the coercive force of the step-aged alloys are remarkably affected by the temperature of the TMT. The analysis of the microstructural features has shown that the morphology of the microstructure is also very much affected by the temperature of the TMT, viz., the size, shape and volume fraction of the two phases, and their composition as well. A detailed interpretation of the differences in the coercive force of the alloys after different heat treatments can not be made at present. This is due to the lack of a detailed model and a formula which clearly gives the controlling parameters of the coercive force. At the same time the compositions of the two phases are not known, and can not be estimated since the shape of the miscibility gap is not known. Therefore the magnetic parameters such as magnetization intensities of the two phases, crystalline anisotropy constants can not be calculated or estimated. Some knowledge of these parameters is needed for detailed interpretation.

SUMMARY AND CONCLUSIONS:

Based on the present study of Fe-Cr-15Co alloys without and with the additions of V, V+Ti, the following conclusions can be drawn.

1) The alloys Fe-28Cr-15Co, Fe-23Cr-15Co-5V, Fe-23Cr-15Co-3V-2Ti (wt. %) consist of an α phase in the as quenched state.

2) γ and σ phases are observed in as quenched state or after isothermal aging, contrary to the implication of the reported phase diagrams in figures 1, 2 and 3.

3) The results of the isothermally aged alloys show that the morphology of the microstructure is very sensitive to the aging temperature, the decomposition process appears to be isotropic at least for 1 hour, and the shape of the miscibility gap is somewhat different for alloys A and B.

4) The thermomagnetic treatment is found to be very effective in elongating the Fe-Co rich α_1 phase particles in these alloys.

5) The magnetic properties of the step-aged alloys are very sensitive to the TMT temperature resulting in different morphologies. Therefore careful temperature control is needed for production of optimum magnetic properties. During step-aging the morphology developed by the TMT essentially does not change, but composition difference between the two phases increases. In order to produce the desired morphology, the step aging interval ΔT should be less than 40°C for the alloy A, and less than 30°C for the alloys B and C. After TMT if ΔT is around 100°C the secondary decomposition may take place spinodally.

6) Continuous cooling is an alternative way to produce optimum magnetic properties. The morphology of the microstructure of the alloys is developed by TMT. Different cooling rates do not essentially alter the microstructure but the composition of the two phases differs with different cooling rates. Low temperature aging subsequent to continuous cooling does not alter the microstructure but increases the difference in the compositions of the two phases.

7) Magnetic domain observations have shown that domain walls lie in the α_2 phase and are pinned by the α_1 phase particles. Domain walls lie along <100> in isothermally aged alloys. Whereas domain walls lie parallel to the applied field in the step-aged or continuously cooled alloys due to the induced anisotropy by TMT. The anisotropy induced by TMT increases during step-aging and continuous cooling. Magnetic domains are narrower for the optimally treated alloys.

8) Magnetization reversal process of the alloys is found to be due to domain wall pinning as Fe-Co rich α_1 particles acting as pinning sites (as opposed to single domain hardening).

ACKNOWLEDGEMENTS:

The author is grateful to Profess Gareth Thomas for his continuous guidance and support throughout this study. The thanks are also due to Professors R.H.Bragg and J.Clarke for their critical review of the manuscript.

Special thanks are due to Dr. Masuo Okada for his guidance, helpful discussions and encouragement. He is also grateful to Professors H. Kaneko and M. Homma for their support, and especially to Mr. T. Minowa for preparing some of the alloys used for this study.

The author acknowledges Etibank, a Governmental Institute of Turkey, for his scholarship during the present work. This research is financially supported by the Department of Energy through the MMRD of the Lawrence Berkeley Laboratory.

REFERENCES:

1. H.Kaneko, M.Homma, K.Nakamura, *AIP Conference Proceedings*, **5**, 1088(1971).
2. R.J.Parker and R.J.Studders, *Permanent Magnets and their applications*, John Wiley & Sons Inc., New York, 1962.
3. B.D.Cullity, *Introduction to Magnetic Materials*, Addison-Wesley, Reading, 1972.
4. H.Kaneko, M.Homma, K.Nakamura, M.Miura, IEEE Trans. Magnetics, **Mag-8**, 347 (1972).
5. M.Okada, Ph.D. Thesis, University of California, Berkeley, May 1978.
6. R.Cremer and I.Pfeiffer, Physica, **80B**, 164 (1975).
7. E.O.Hall and S.H.Algie, Metallurgical Reviews, **11**, 61 (1966).
8. A.Higuchi, M.Kamiya and K.Suzuki, *Proceedings of 3rd European conference of Hard Magnetic Materials*, Amsterdam, 201, 1974.
9. H.Kaneko, M.Homma, T.Fukunaga and M.Okada, IEEE Trans. magnetics, **Mag-11**, 1440 (1975).
10. H.Kaneko, M.Homma and T.Minowa, ibid., **Mag-12**, 177 (1976).
11. M.McCaig, ibid., **Mag-11**, 1443 (1975).
12. G.Y.Chin, J.T.Plewes and B.C.Wonsiewicz, J.Appl.Phys., **49**, 2046 (1978).
13. E.C.Stoner and E.P.Wohlfarth, Phil. Trans. of Royal Soc. London, **240(A)** (1948).

14. P.B.Hirsch et al., *Electron Microscopy of Thin Crystals*, Chap. 16. Butterworths, London, 1965.

15. J.P.Jakubovics in *Electron Microscoy in Materials Science*, Part IV, Commission of the european Communities, 1975.

16. H.Kaneko, M.Homma, K.Nakamura, M.Okada, G.Thomas, IEEE Trans. Magnetics, **Mag-13**, 1325 (1977).

17. M.Okada, G.Thomas, H.Kaneko,M.Homma, IEEE Trans. Magnetics, in press.

18 H.Kaneko, M.Homma, T.Minova, unpublished work.

19. H.Kaneko, M.Homma, unpublished work.

20. K.J.DeVos in *Magnetism and Metallurgy*, A.E.Berkowitz and E.Kneller eds., Vol.1, Chap. 9, Academic Press, New York, 1969.

21. J.D.Livingston and D.L.Martin, J. Appl. Phys., **48**, 1350 (1977).

22. H.Kaneko, M.Homma, M.Okada, S.Nakamura and N.Ikuata, AIP Cong. Proc., **29**, 620 (1975).

23. M.Okada, M.Homma, H.Kaneko and G.Thomas, 34th Ann. Proc. EMSA, 606 (1976).

24. J.W.Cahn, J.Appl. Phys., **34**, 3581 (1963).

25. P.G.Shewmon in *Transformation in Metals*, Mc Graw Hill, New York, 1969.

26. K.J.DeVos in *The Relationship between Microstructure and Magnetic Properties of Alnico alloys*, Thesis, University of Eindhoven, 1966.

27. C.P.Bean and J.D.Livingston, J. Appl. Phys., **30**, 1205 (1959).

28. R.S.Tebble and D.J.Craik in *Magnetic Materials*, John Wiley & Sons, London, 1969.

29. E.A.Wesbitt and H.J.Williams, Phys. Rev., **80**, 112 (1950).

30. W.Andrä, Ann. Phys., **19**, 10 (1956).

31. L.F.Bates et al., Proc. Phys. Soc., **79**, 970 (1962).

32. D.J.Craik and R.S.Tebble, in *Ferromagnetism and Ferromagnetic Domains*, North-Holland Publis. Co., Amsterdam, 1965.

33. D.J.Craik and R.Lone, Brit. J. Appl. Phys., Ser. 2, **2** (1969).

34. S.Mahajan, private communication.

35. M.Kersten, in *Grundlagen einer Theorie der Ferromagnetishen Hysterese und Koerzitivkraft*, Verlag Hirzel, Leipzig, 1943.

36. E.Schwabe, Ann. Phys., **11**, 99 (1952).

FIGURE CAPTIONS:

Figure 1. Vertical section of the Fe-Cr-Co phase diagram at 15 wt.% Co. (Reference 10)

Figure 2. Vertical section of the Fe-Cr-Co phase diagram at 15 wt.%Co and 5 wt.% V. (Reference 10)

Figure 3. Vertical section of the Fe-Cr-CO phase diagram at 15 wt.%Co, 3 wt.% V and 2 wt.% Ti. (Reference 10)

Figure 4. Bright Field (B.F.) micrographs of the alloys in as quenched state. a) Fe-28Cr-15Co (wt.%) alloy A. b) Fe-23Cr 15Co-5V (wt%) alloy B. c) Fe-23Cr-15Co-3V-2Ti (wt.%) alloy C.

Figure 5. B.F. micrograph taken from the step-aged alloy C thermomagnetically treated at 640°C for 1 hour, showing γ grains.

Figure 6. Electron micrographs taken from the alloy A aged at 640°C for 1 hour.

Figure 7. B.F. micrographs of the step-aged alloy A thermomagnetically treated at 670°C for 1 hour.

Figure 8. B.F. micrographs taken from the isothermally aged alloy B for 1 hour at a) 660°C, b) 650°C, c) 640°C and d) 630°C.

Figure 9. B.F. micrographs taken from the isothermally aged alloy A for 1 hour at a) 670°C, b) 650°C, c) 640°C.

Figure 10. B.F. micrograph, taken from the alloy B a) after aging at 650°C for 1 hour (100) foil orientation. b) after TMT at 650°C for 1

hour, foil orientation parallel to the applied field direction.

Figure 11. Schematic diagrams of the step-aging method for the alloys A, B and C.(The specimens thermomagnetically treated at 630°C were not step-aged at 620°C.)

Figure 12. Magnetic properties of the step-aged alloy A vs. the temperature of the TMT.

Figure 13. Magnetic properties of the step-aged alloy B vs. the temperature of the TMT.

Figure 14. Magnetic properties of the step-aged alloy C vs. the temperature of TMT.

Figure 15. B.F. micrographs taken from the step-aged alloy B after thermomagnetic treatment for 1 hour at a) 660°C (H_c~420 Oe), b) 650°C (H_c~520 Oe), c) 640°C (H_c~370 Oe), d) 630°C (H_c~80 Oe).

Figure 16. B.F. micrographs taken from the step-aged alloy A after thermomagnetic treatment for 1 hour at a) 670°C (H_c~240 Oe), b) 660°C (H_c~610 Oe), c) 650°C (H_c~580 Oe), d) 640°C (H_c~330 Oe).

Figure 17. B.F. micrographs taken from the step-aged alloy C after thermomagnetic treatment for 1 hour at a) 660°C (H_c~550 Oe), b) 650°C (H_c~580 Oe), c) 640°C (H_c~390 Oe), d) 630°C (H_c~150 Oe).

Figure 27. Fresnel micrographs taken from the alloy B aged at 650°C showing that the domain wall is pinned by the α_1 particles.

Figure 28. Fresnel micrographs taken from the thermomagnetically treated alloy B at 650°C for 1 hour. a) parallel to the applied field, b) perpendicular to the applied field.

Figure 29. Foucault micrographs of the continuously cooled alloy B cooled at a rate of 1°C/min. after thermomagnetic treatment at 650°C for 1 hour ($H_t \sim 220$ Oe).

Figure 30. Fresnel [(a), (b)] and Foucault micrographs [(c) and (d)] of the step-aged alloy after TMT at 650°C for 1 hour ($H_t \sim 520$ Oe).

Figure 31. Foucault micrograph of the step-aged alloy B thermomagnetically treated at 650°C for 1 hour.

Figure 32. Foucault micrographs taken from the step-aged alloy B thermomagnetically treated at 640°C for 1 hour, showing the domains are elongated along the same directions across two grains with different crystal orientations.

Figure 33. Fresnel micrographs of the optimally step-aged alloy B, and its figurative interpretation of the domain configuration.

Figure 34. Fresnel micrographs of the optimally step-aged alloy C, showing the domain configuration in foil perpendicular to the applied field.

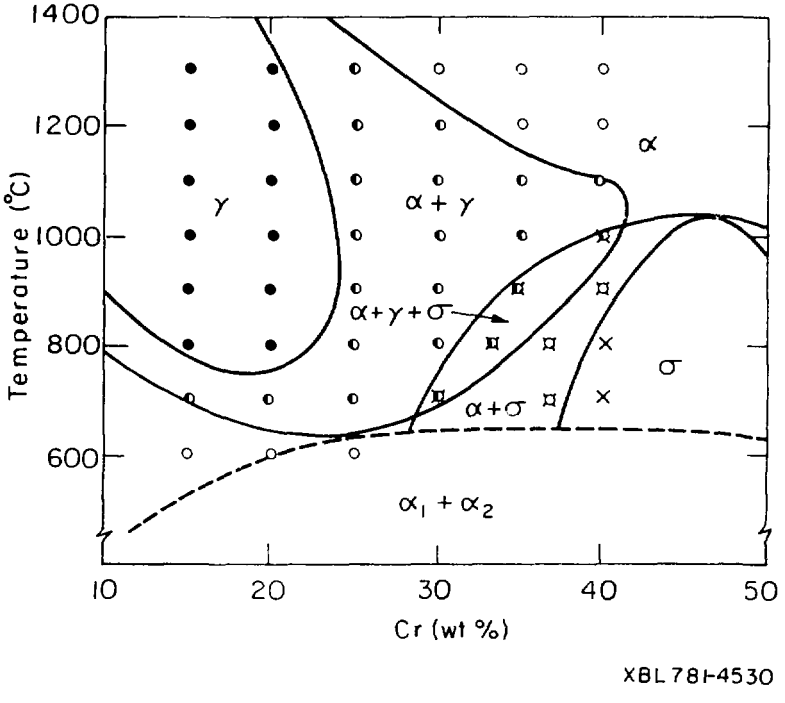
1400
1200
1000
800
600
Temperature (°C)
10
20
30
40
50
Cr (wt %)
γ
α + γ
α
α+γ+σ
σ
α+σ
α1 + α2
XBL 781-4530

Fig.I

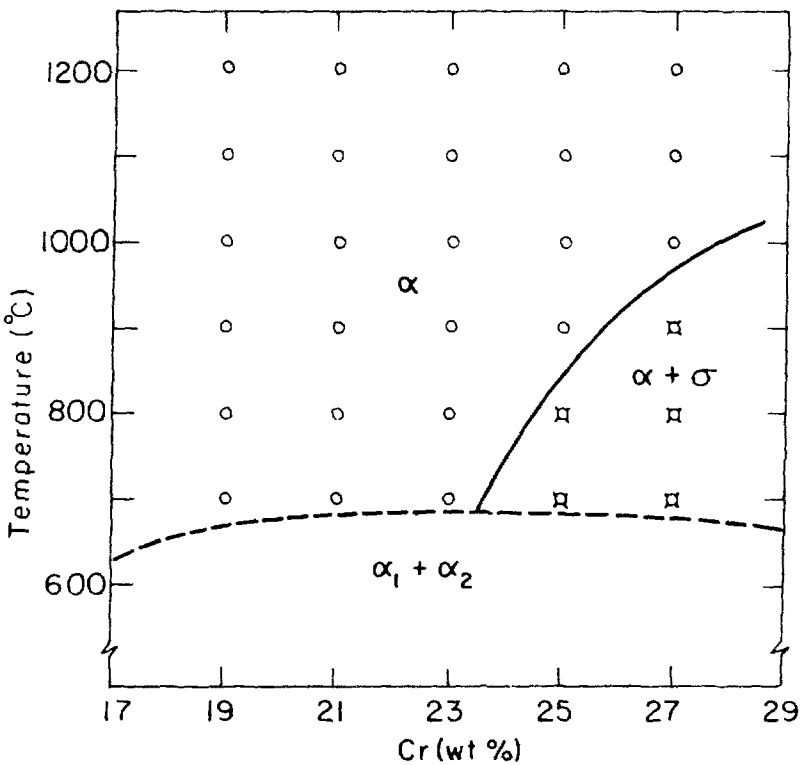
1200
1000
800
600
Temperature (°C)
α
α + σ
α1 + α2
17
19
21
23
25
27
29
Cr (wt %)
XBL 781-4532

Fig.2

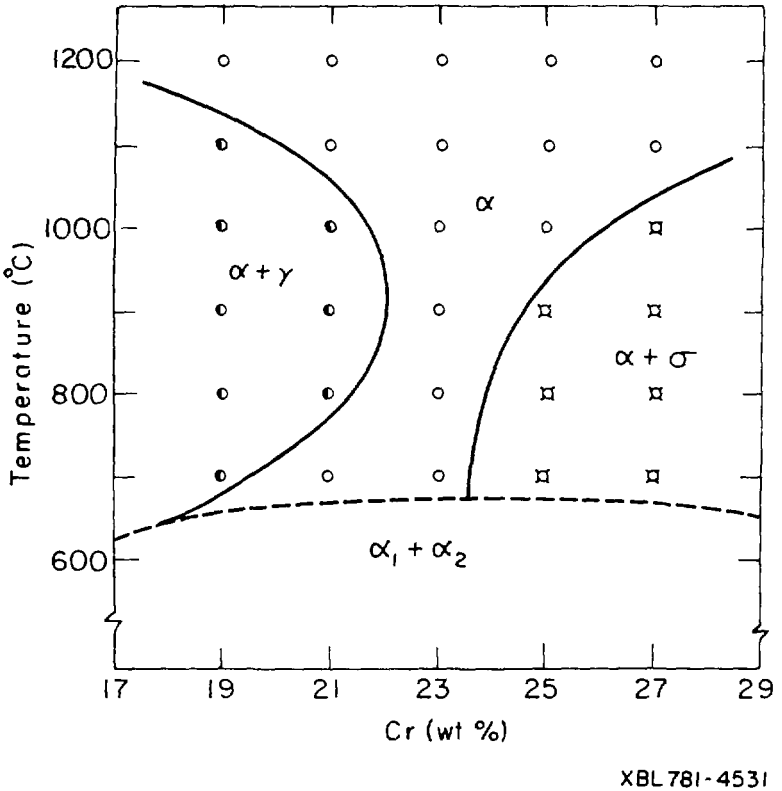
1200
1000
800
600
Temperature (°C)
α
α + γ
α + σ
α1 + α2
17
19
21
23
25
27
29
Cr (wt %)
XBL 781-4531

Fig.3

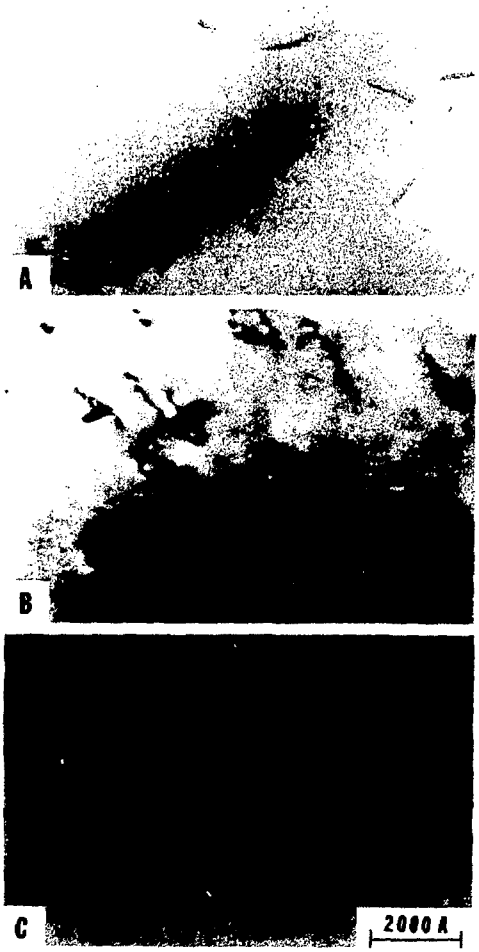

XBB 785 5394

Fig. 4

XBB 785 5393

Fig. 5

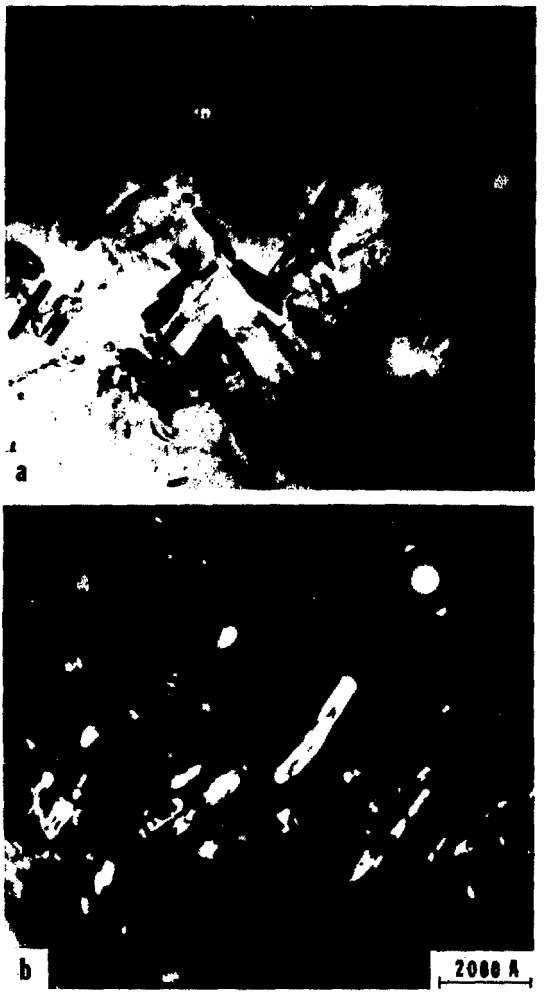

XBB 785 5395

Fig. 6

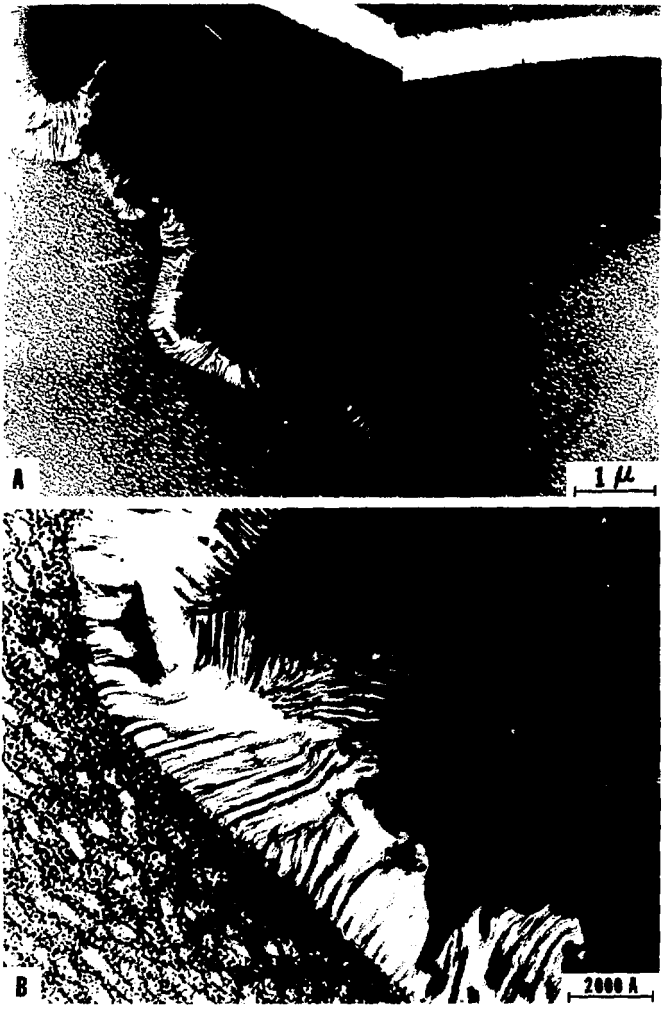

XBB 785 5397

Fig. 7

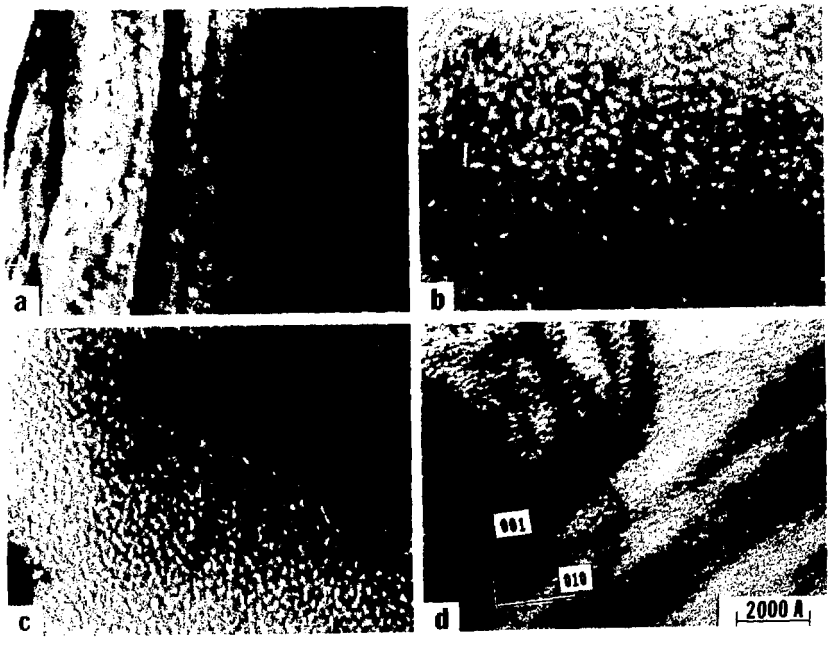

XBB 7710 10356

Fig. 8

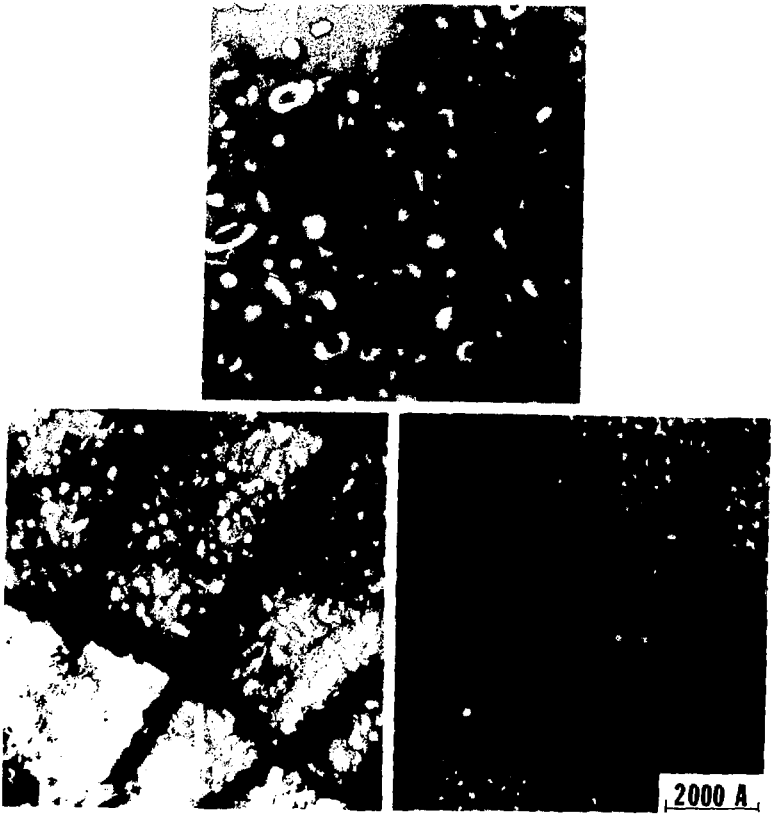

XBB 785 5973

Fig. 9

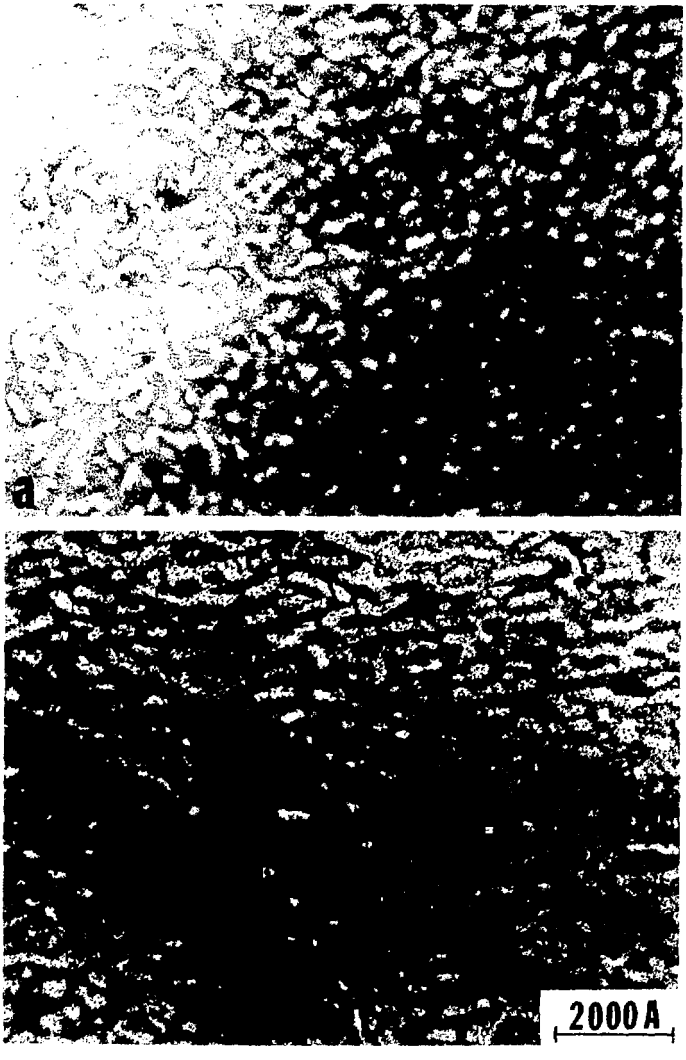

XBB 785 5972

Fig. 10

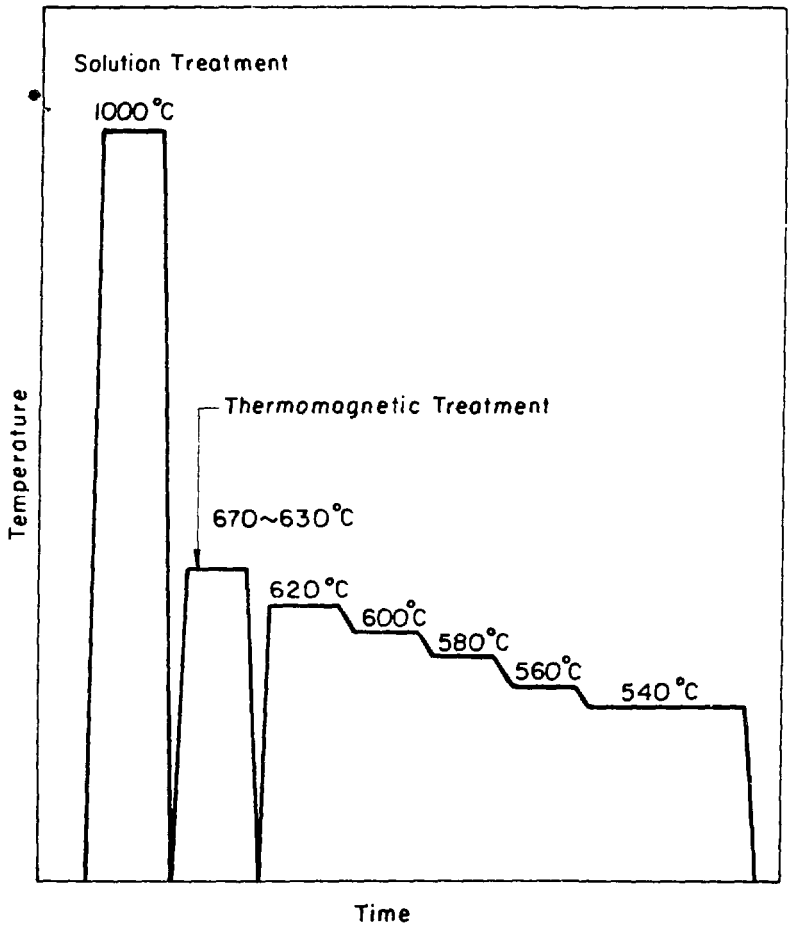

XBL 7710-6296

Fig.11

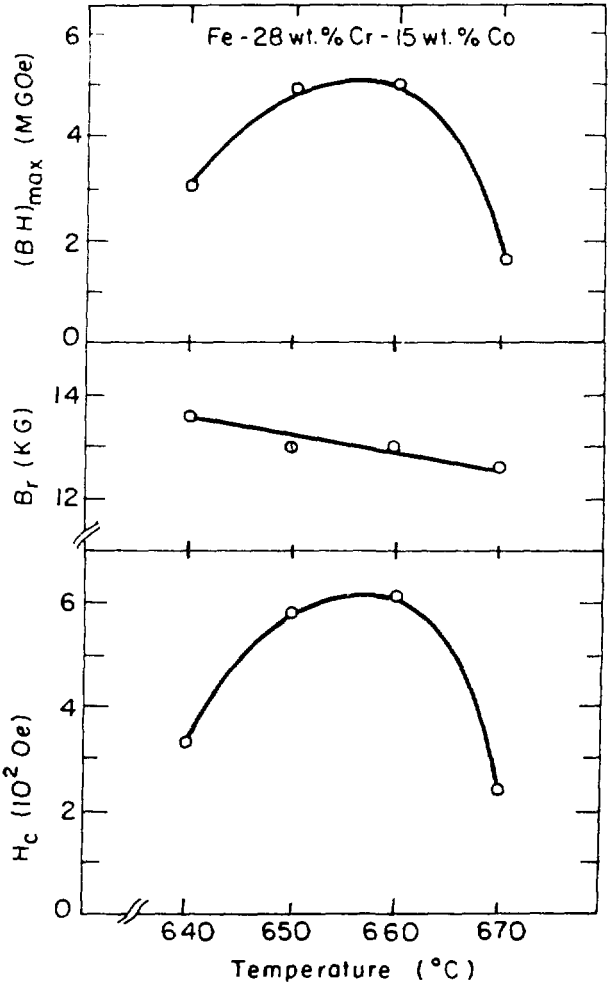
Fe - 28 wt.% Cr - 15 wt.% Co
$(BH)_{max}$ (MGOe)
B_r (KG)
H_c (10^2 Oe)
Temperature (°C)
640
650
660
670
XBL7710-6301

Fig.12

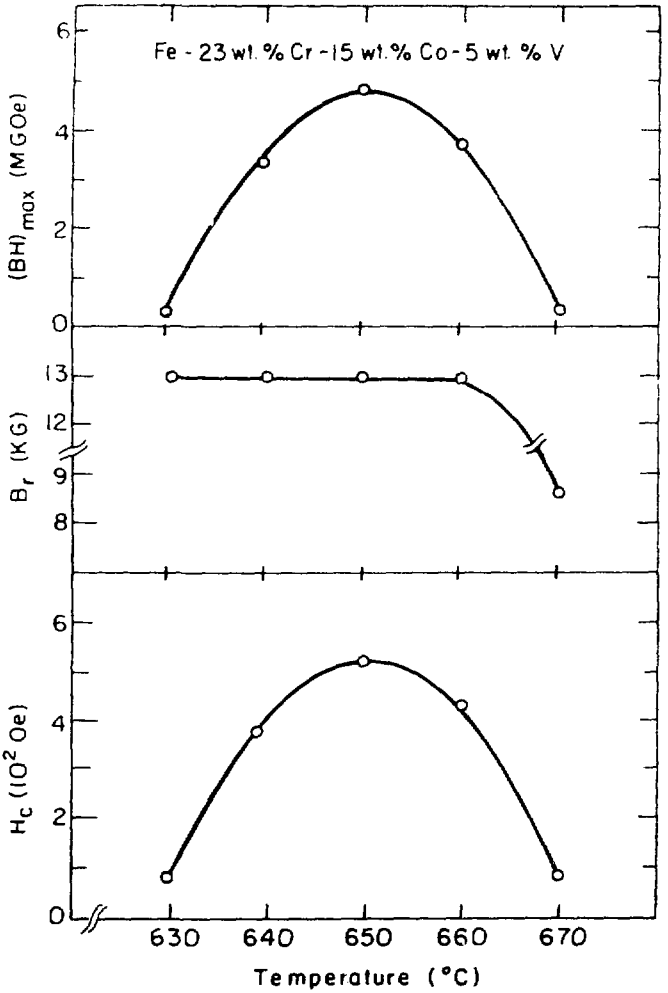
Fe - 23 wt. % Cr - 15 wt. % Co - 5 wt. % V
$(BH)_{max}$ (MGOe)
B_r (KG)
H_c (10^2 Oe)
Temperature (°C)
630
640
650
660
670
XBL 7710-6300

Fig.13

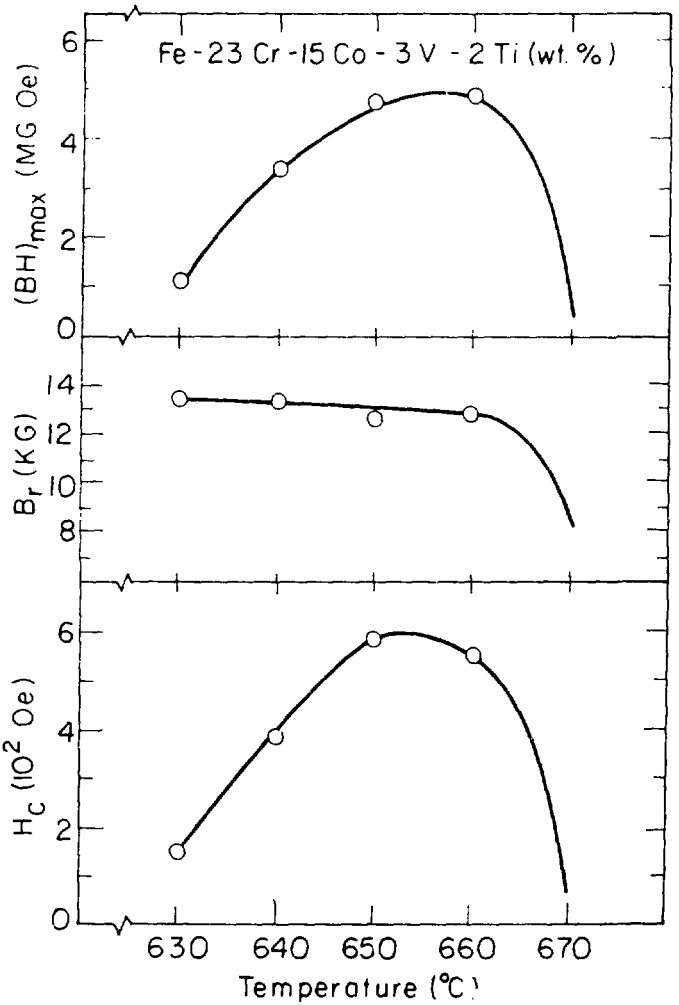

XBL 781-4534

Fig.14

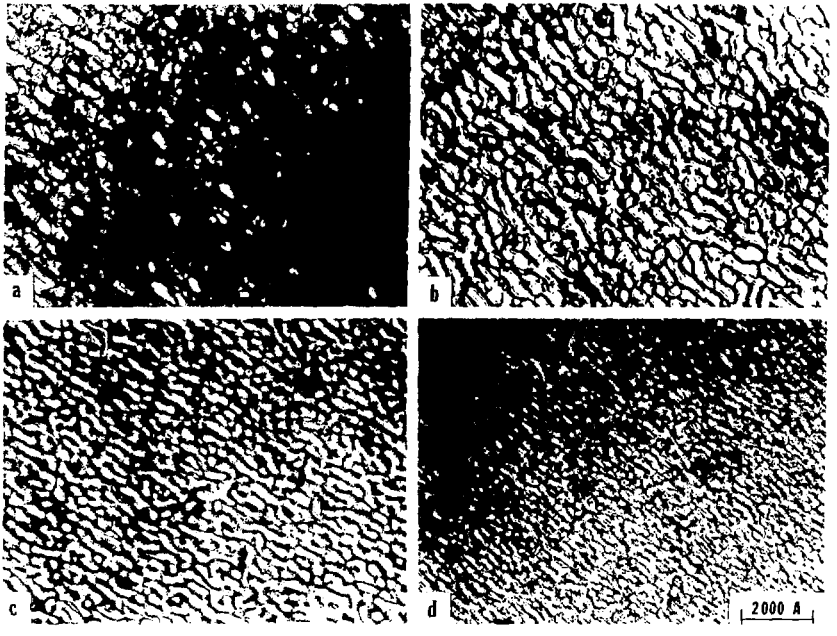

XBB 779 9128

Fig. 15

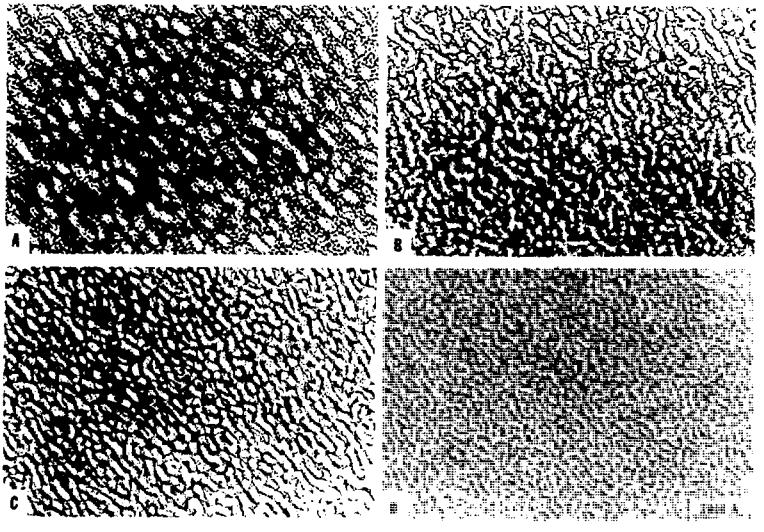

XBB 785 5398

Fig. 16

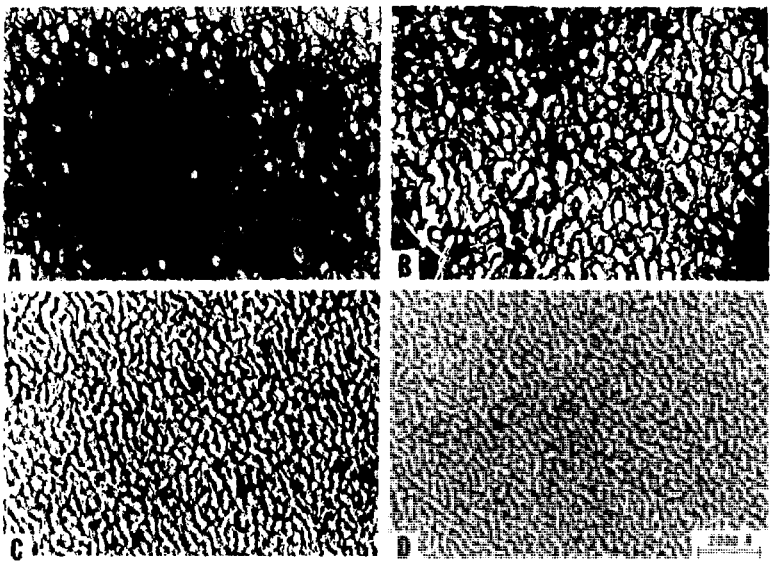

XBB 785 5399

Fig. 17

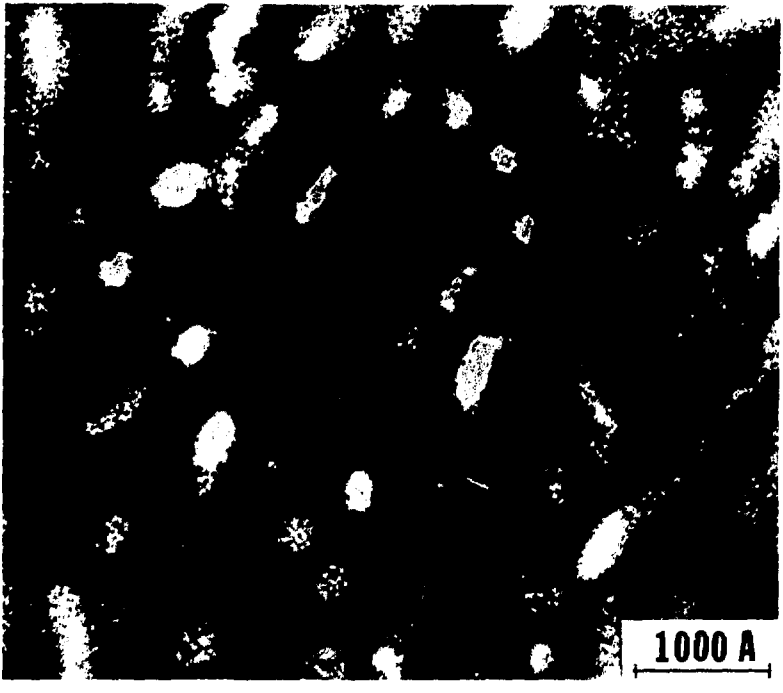

XBB 785 5392

Fig. 18

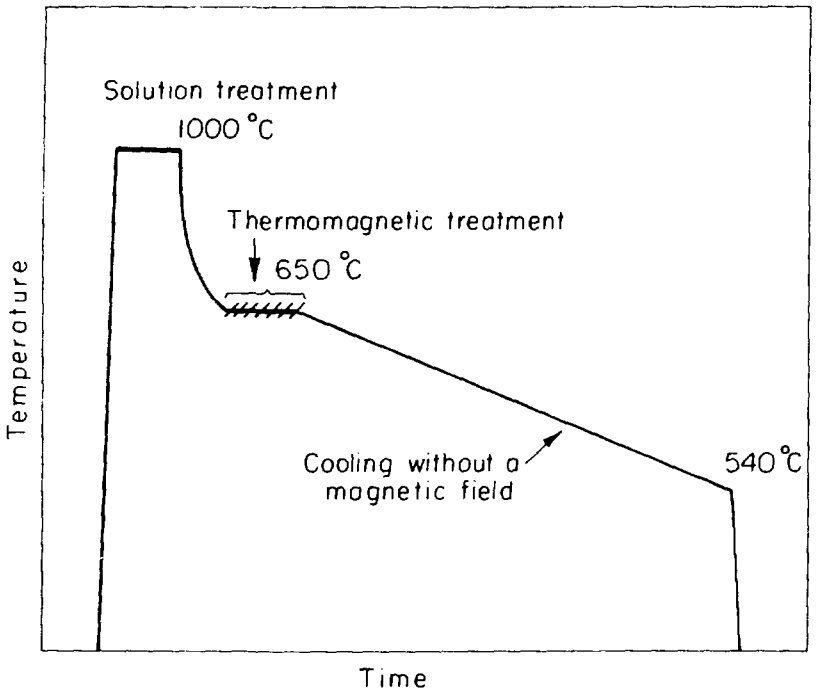

XBL 781-4533

Fig.19

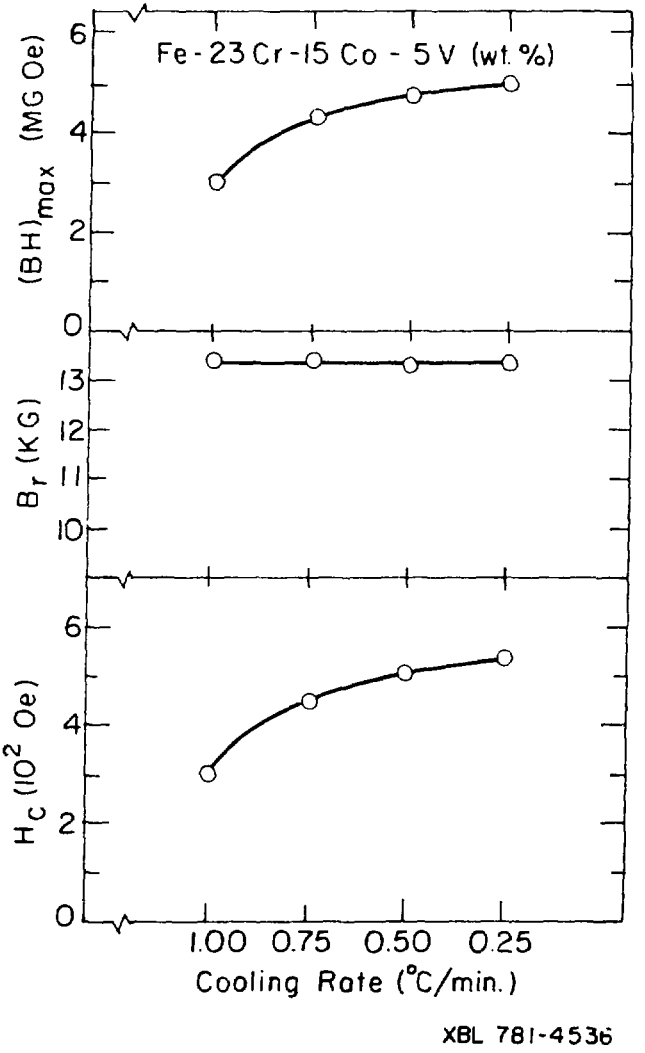
Fe - 23 Cr - 15 Co - 5 V (wt. %)
$(BH)_{max}$ (MG Oe)
6
4
2
0
B_r (KG)
13
12
11
10
H_c (10^2 Oe)
6
4
2
0
1.00 0.75 0.50 0.25
Cooling Rate (°C/min.)
XBL 781-4536

Fig.20

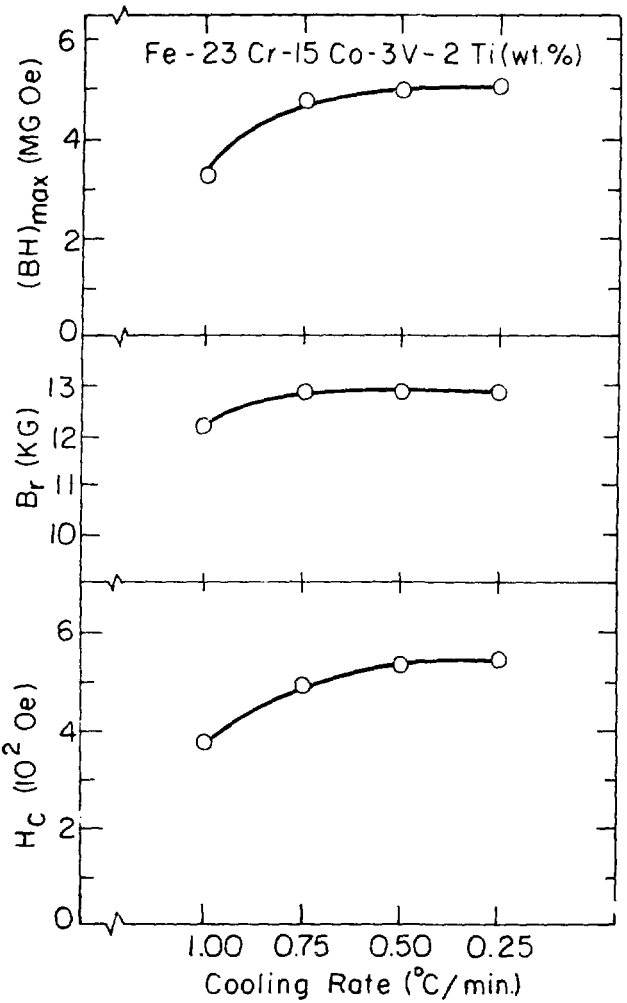
Fe - 23 Cr - 15 Co - 3V - 2 Ti (wt.%)
$(BH)_{max}$ (MG Oe)
6
4
2
0
B_r (KG)
13
12
11
10
H_c (10^2 Oe)
6
4
2
0
1.00
0.75
0.50
0.25
Cooling Rate (°C/min.)
XBL 781-4535

Fig.21

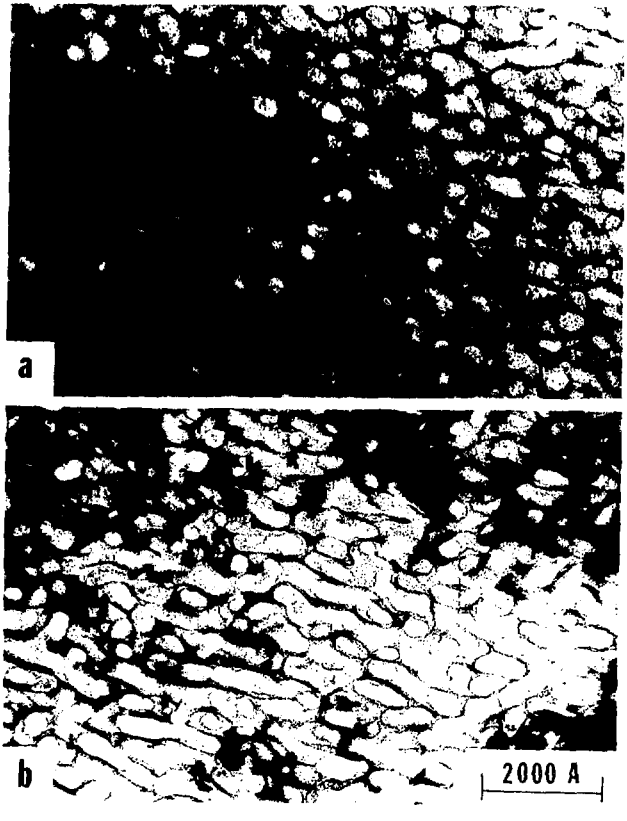

XBB 779 9130

Fig. 23

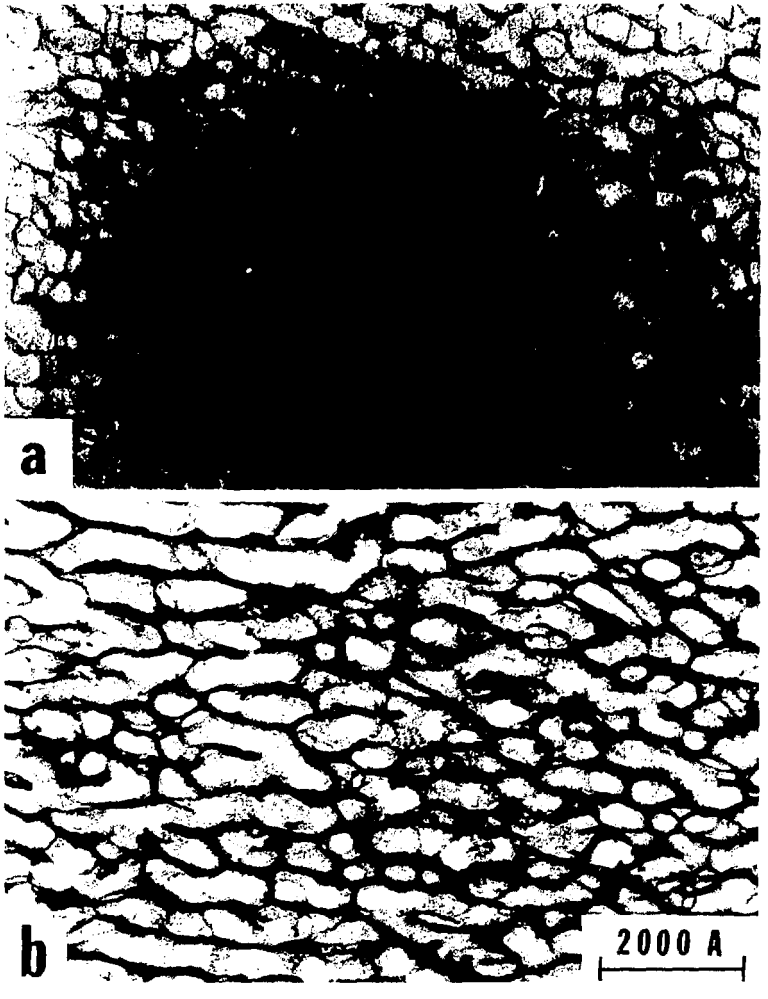

XBB 785 5391

Fig. 23

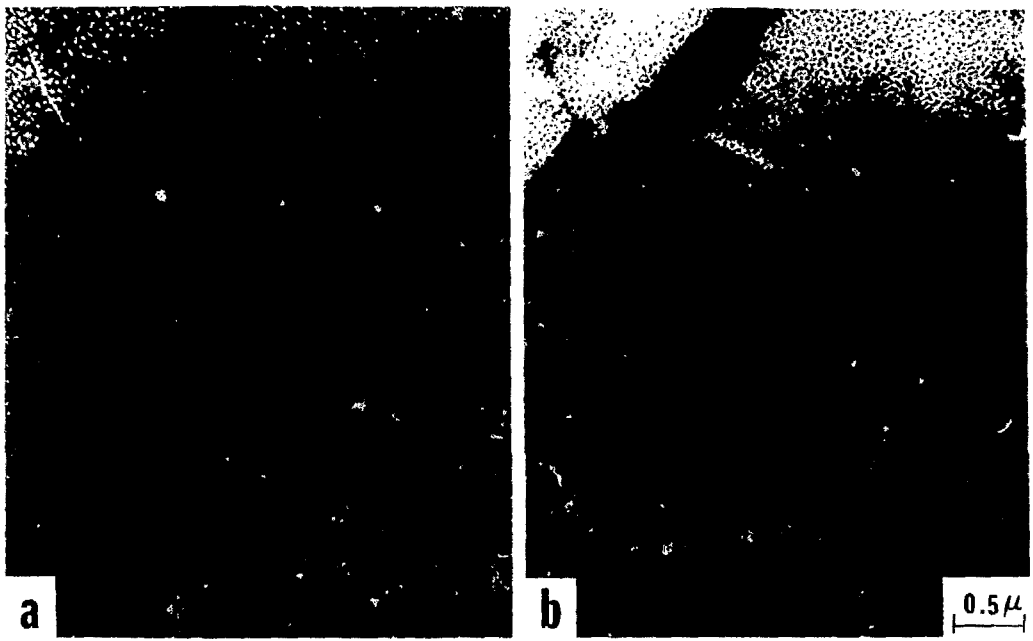

XBB 779 9125A

Fig. 24

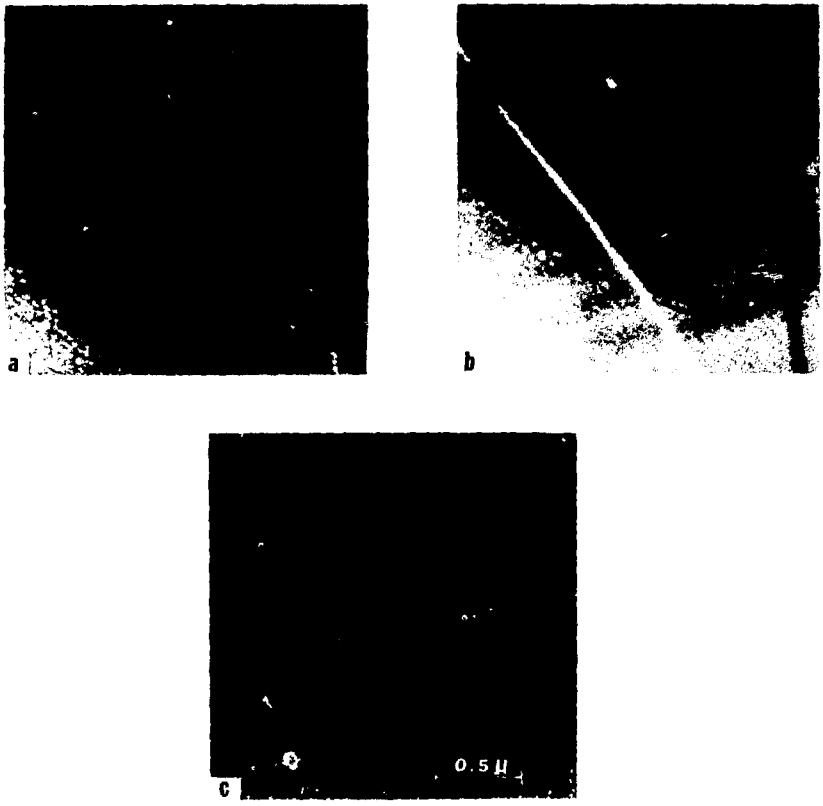

XBB 775 5250

Fig. 25

XBB 7710 10358

Fig. 26

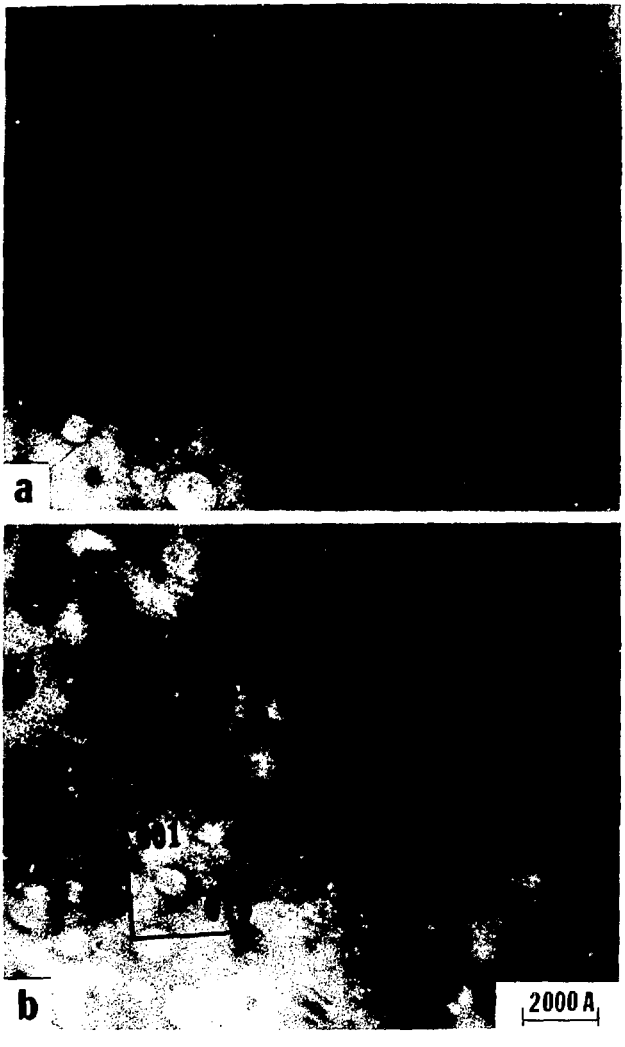

XBB 779 9126A

Fig. 27

XBB 781 451

Fig. 28

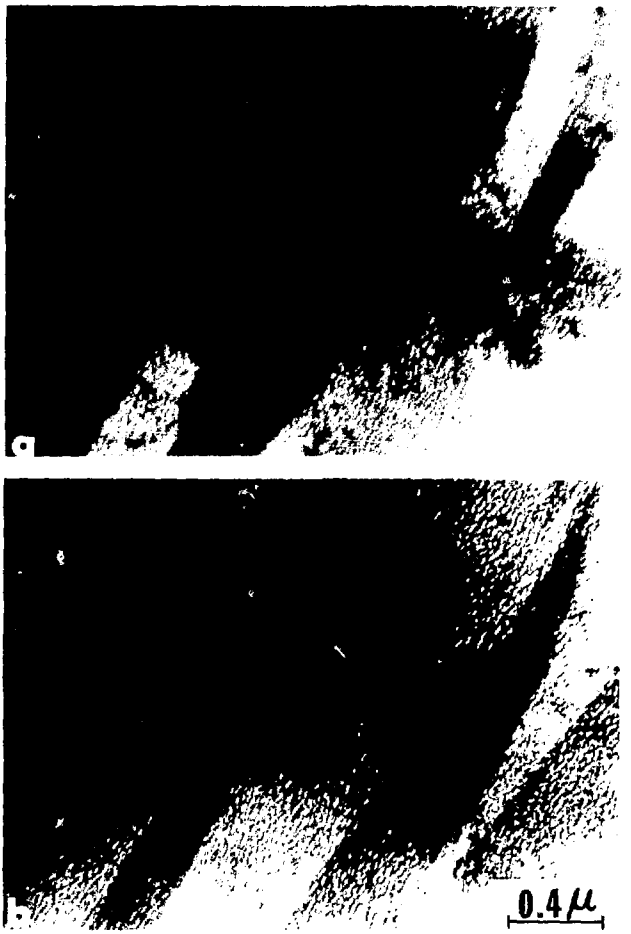

XBB 7710 10357

Fig. 29

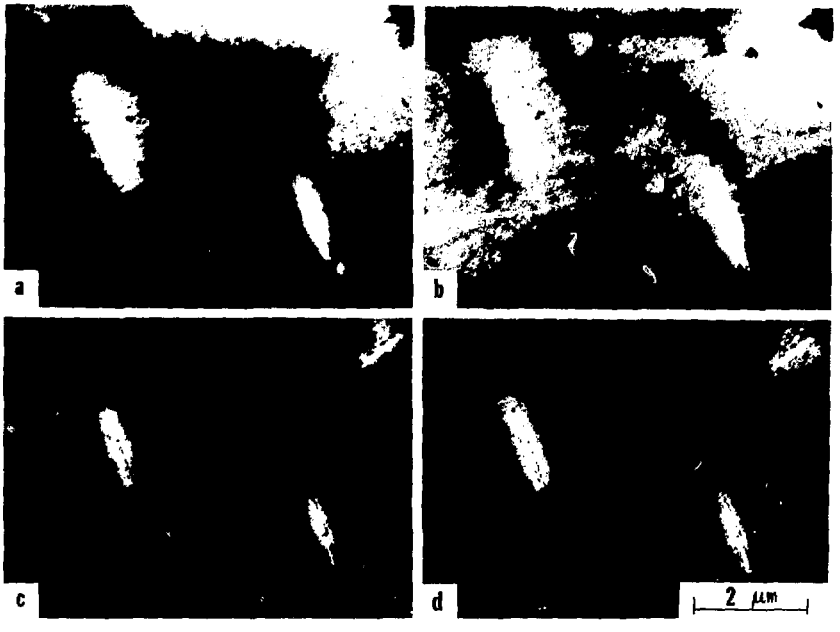

XBB 779 9129

Fig. 30

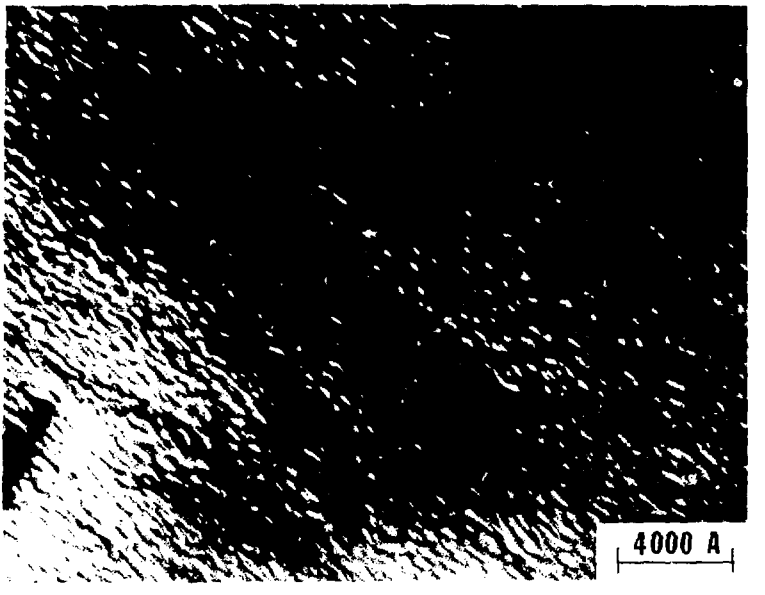

XBB 779 9127

Fig. 31

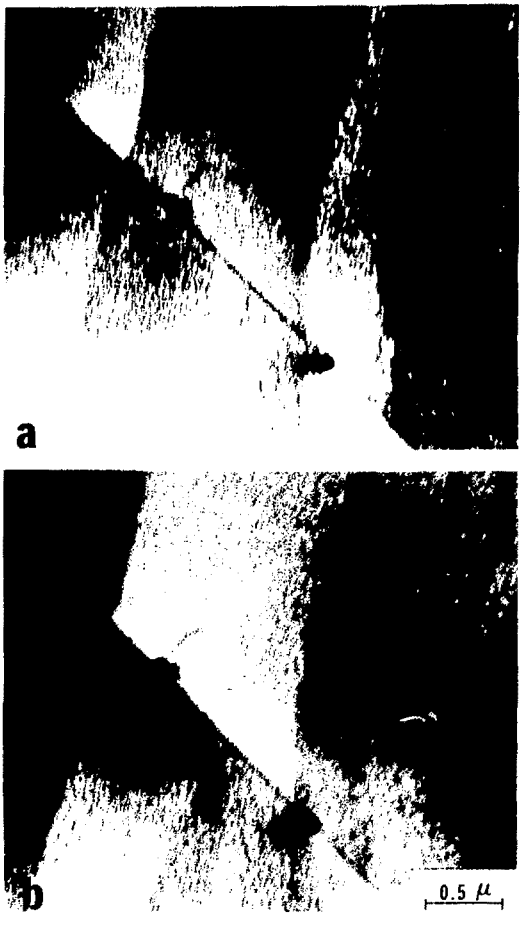

XBB 7710 10359

Fig. 32

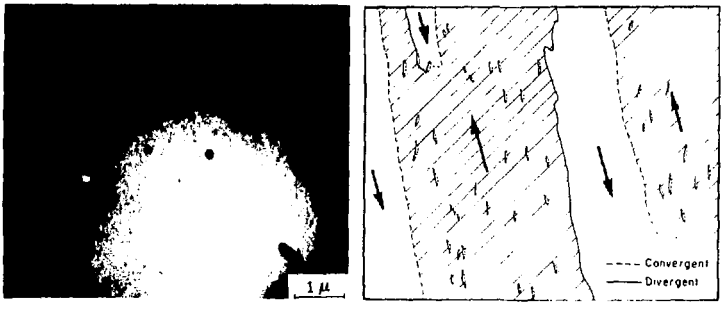

XBB 785 5390

Fig. 33

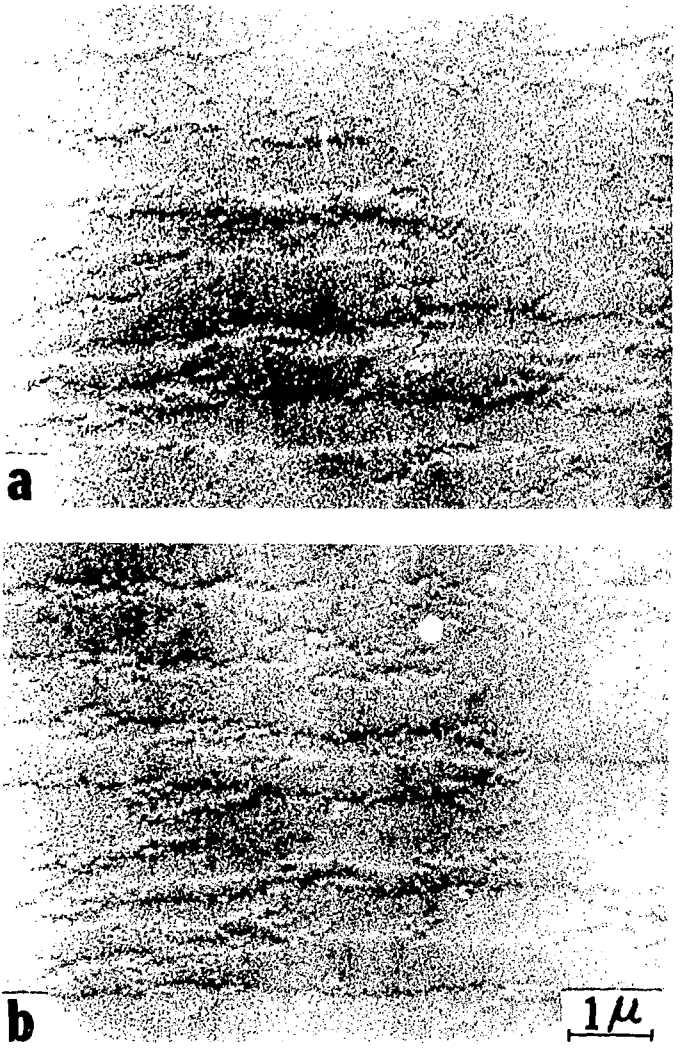

XBB 781 450

Fig. 34